Ultraviolet radiation modelling from ground-based and satellite measurements on Reunion Island, southern tropics

Kévin Lamy, Thierry Portafaix, Colette Brogniez, Sophie Godin-Beekmann, Hassan Bencherif, Béatrice Morel, Andrea Pazmino, Jean-Marc Metzger, Frédérique Auriol, Christine Deroo, et al.

Atmos. Chem. Phys., 18, 227–246, 2018
https://doi.org/10.5194/acp-18-227-2018

Atmospheric Chemistry and Physics
Open Access
EGU

Ultraviolet radiation modelling from ground-based and satellite measurements on Reunion Island, southern tropics

Kévin Lamy[1], Thierry Portafaix[1], Colette Brogniez[2], Sophie Godin-Beekmann[3], Hassan Bencherif[1,4], Béatrice Morel[5], Andrea Pazmino[3], Jean Marc Metzger[6], Frédérique Auriol[2], Christine Deroo[2], Valentin Duflot[1], Philippe Goloub[2], and Charles N. Long[7]

[1]LACy, Laboratoire de l'Atmosphère et des Cyclones (UMR 8105 CNRS, Université de La Réunion, Météo-France), Saint-Denis, Reunion Island, France
[2]Laboratoire d'Optique Atmosphérique (LOA), Université Lille 1 Sciences et Technologies, Villeneuve d'Ascq, France
[3]Laboratoire Atmosphères, Milieux, Observations Spatiales, Service d'Aéronomie (LATMOS), CNRS, Institut Pierre Simon Laplace, Pierre et Marie Curie University, Paris, France
[4]School of Chemistry and Physics, University of KwaZulu Natal, Durban, South Africa
[5]Laboratoire d'Energétique, d'Electronique et Procédés (LE2P), Université de la Réunion, Saint-Denis, Reunion Island, France
[6]Observatoire des Sciences de l'Univers Réunion (OSU-R), UMS 3365, Université de la Réunion, Saint-Denis, Reunion Island, France
[7]National Oceanographic and Atmospheric Administration, Earth System Research Laboratory, Boulder, Colorado, USA

Correspondence: Kévin Lamy (kevin.lamy@univ-reunion.fr)

Received: 20 June 2017 – Discussion started: 24 July 2017
Revised: 30 October 2017 – Accepted: 9 November 2017 – Published: 9 January 2018

Abstract. Surface ultraviolet radiation (SUR) is not an increasing concern after the implementation of the Montreal Protocol and the recovery of the ozone layer (Morgenstern et al., 2008). However, large uncertainties remain in the prediction of future changes of SUR (Bais et al., 2015). Several studies pointed out that UV-B impacts the biosphere (Erickson et al., 2015), especially the aquatic system, which plays a central part in the biogeochemical cycle (Hader et al., 2007). It can affect phytoplankton productivity (Smith and Cullen, 1995). This influence can result in either positive or negative feedback on climate (Zepp et al., 2007).

Global circulation model simulations predict an acceleration of the Brewer-Dobson circulation over the next century (Butchart, 2014), which would lead to a decrease in ozone levels in the tropics and an enhancement at higher latitudes (Hegglin and Shepherd, 2009). Reunion Island is located in the tropics (21° S, 55° E), in a part of the world where the amount of ozone in the ozone column is naturally low. In addition, this island is mountainous and the marine atmosphere is often clean with low aerosol concentrations. Thus, measurements show much higher SUR than at other sites at the same latitude or at midlatitudes. Ground-based measurements of SUR have been taken on Reunion Island by a Bentham DTMc300 spectroradiometer since 2009. This instrument is affiliated with the Network for the Detection of Atmospheric Composition Change (NDACC). In order to quantify the future evolution of SUR in the tropics, it is necessary to validate a model against present observations. This study is designed to be a preliminary parametric and sensitivity study of SUR modelling in the tropics.

We developed a local parameterisation using the Tropospheric Ultraviolet and Visible Model (TUV; Madronich, 1993) and compared the output of TUV to multiple years of Bentham spectral measurements. This comparison started in early 2009 and continued until 2016.

Only clear-sky SUR was modelled, so we needed to sort out the clear-sky measurements. We used two methods to detect cloudy conditions: the first was based on an observer's hourly report on the sky cover, while the second was based on applying Long and Ackerman (2000)'s algorithm to broadband pyranometer data to obtain the cloud fraction and then discriminating clear-sky windows on SUR measurements.

Long et al. (2006)'s algorithm, with the co-located pyranometer data, gave better results for clear-sky filtering than the observer's report.

Multiple model inputs were tested to evaluate the model sensitivity to different parameters such as total ozone column, aerosol optical properties, extraterrestrial spectrum or ozone cross section. For total column ozone, we used ground-based measurements from the SAOZ (Système d'Analyse par Observation Zénithale) spectrometer and satellite measurements from the OMI and SBUV instruments, while ozone profiles were derived from radiosoundings and the MLS ozone product. Aerosol optical properties came from a local aerosol climatology established using a Cimel photometer. Since the mean difference between various inputs of total ozone column was small, the corresponding response on UVI modelling was also quite small, at about 1 %. The radiative amplification factor of total ozone column on UVI was also compared for observations and the model. Finally, we were able to estimate UVI on Reunion Island with, at best, a mean relative difference of about 0.5 %, compared to clear-sky observations.

1 Introduction

Ozone recovery prevented a significant increase in SUR level (e.g Morgenstern et al., 2008; van Dijk et al., 2013; Newman et al., 2009...). However, large uncertainties remain in the prediction of the future changes of SUR (Bais et al., 2015). Overexposure to this radiation is the main cause of the development of non-melanoma and melanoma skin cancers. Non-melanoma skin cancer is induced by chronic exposure and melanoma is induced by repeated burning and chronic exposure (Matsumura and Ananthaswamy, 2004). Holick et al. (1980) studied the beneficial effect of UV radiation on health through the synthesis of pre-vitamin D and numerous studies have assessed the balance between benefits and risks. McKenzie et al. (2009) looked at the relation between erythemal-weighted UV (McKinlay and Diffey, 1987) and vitamin-D-weighted UV (MacLaughlin et al., 1982). This work showed that, during summer at midlatitudes, vitamin D can be produced in a few minutes while avoiding the skin damage that occurs after an hour of exposure; of course this depends on the skin area exposed. Behavioural studies have also been conducted in order to understand human activities in relation to UV intensity. Participating in outdoor sports activities without sufficient solar protection has been shown to increase the risk of developing skin lesions in childhood (Mahé et al., 2011). Tourism in northern midlatitude cities in summer can also present a non-negligible risk of skin cancer (Mahé et al., 2013). UV exposure and sun-protective practices during childhood were also investigated in New Zealand (Wright et al., 2007), and differences in children's exposure were explained by their different activities. Sunburn risks among children and outdoor workers were evaluated on Reunion Island and in South Africa. High values of cumulative daily ambient solar UV radiation were found for the three sites studied (Wright et al., 2013).

Total solar irradiance at the top of the atmosphere is, of course, the source of surface UV radiation. Its intensity varies directly with sun radiative intensity. The sun has an 11-year solar cycle period (Willson and Hudson, 1991) which has a direct influence on total solar irradiance at the top of the atmosphere. Total solar irradiance at the top of the atmosphere is also modulated by the variation in Earth's orbital parameters, which should be taken into account in very long-term climate studies but can be neglected in multi-decadal studies such as ours.

SUR is attenuated by absorbing and scattering processes in the atmosphere from the top of the atmosphere to the surface. By investigating SUR variability from 1 year of ground-based measurements, McKenzie et al. (1991) showed that the dominant variation of SUR was linked to SZA, while attenuation by clouds could exceed 50 % and a total ozone column reduction of 1 % could induce an increase in SUR of 1.25 ± 0.20 %.

Due to the depletion of the ozone layer by human-made halogenated substances and the significant impact of ozone on climate change, a major observing programme was set up to monitor atmospheric ozone in the last decades. The latest assessment of the state of the ozone layer (WMO, 2014) reported the end of the stratospheric ozone decline since the end of the 1990s, with a stabilisation of ozone levels at about 2 % below those observed in the early 1980s. However, global circulation model simulations predict an acceleration of the Brewer-Dobson circulation over the next century (Butchart, 2014), which would lead to a decrease in ozone levels in the tropics and an enhancement at higher latitudes (Hegglin and Shepherd, 2009). Clouds and aerosols are also being intensively investigated, given their role in the climate energy budget and the fact that their radiative forcing remains the main uncertainty for climate studies (Boucher et al., 2013). They also are the main uncertainty factors in the future projections of the solar UV irradiance (Bais et al., 2015). Global maps of UV-absorbing aerosols were derived by Herman et al. (1997). Later Krzyścin and Puchalski (1998) showed that a 10 % decrease in aerosol optical thickness (AOT) at 550 nm induced a ~ 1.5 % increase in UV erythemal daily dose. More recently Kazadzis et al. (2009) investigated the aerosol forcing efficiency in the UVA region, between 325nm and 340nm and found a mean reduction of irradiance of 15.2 % per unit of AOT slant column at 340 nm during autumn. Correa et al. (2013) looked at the influence of aerosol properties on projected changes in clear-sky erythemal UV doses throughout the 21st century. It has been shown that clouds usually reduce SUR variability (Bais et al., 1993; Calbó et al., 2005), but broken clouds can also enhance it under specific conditions (Mayer et al., 1998).

Those three time-evolving parameters being important sources of variability of UV radiation, we need to better understand their effects on surface UV. Radiative transfer modelling plays a key role in deducing UV evolution over the next century, but it needs to take into account a fair projection of those parameters. Climate models associated with radiative transfer models or empirical methods have been used to assess SUR evolution over the coming century. Bais et al. (2011) and McKenzie et al. (2011) respectively found decreases of 12 and 20 % in UVI at high latitude, 3 to 5 % at midlatitudes and increases of 1 to 3 % in the tropics. These projections depend strongly on the evolution of future climate, and Butler et al. (2016) presented the complexities associated with future ozone change and therefore surface UV change.

The ultraviolet index (UVI) (WHO, 2002) is one of the most common parameters used to investigate the impact of SUR on human health. It is the weighted integral of the ultraviolet irradiance between 280 and 400 nm, with the weight depending on the human skin's response to erythema determined by McKinlay and Diffey (1987). UVI modelling was investigated thoroughly by Badosa et al. (2007), who tested multiple inputs and compared the results to observations at four different sites (Lauder, 45.04° S; Boulder, 40.01° N; Mauna Loa, 19.53° N; and Melbourne, 37.63° S). They found mean relative differences in UVI between the model and observations ranging from 10 % to less than 0.1 %.

Following these studies, the present work tries to improve the understanding of surface UV variability in the southern tropical region, a sensitive area where very few studies have been conducted. This article is intended to improve surface UV modelling by analysing the model sensitivity to different inputs. Six years of ground surface UV measurements made with a Bentham DTMc300 spectroradiometer are analysed in comparison to ozone, cloud and aerosol data derived from ground and satellite measurements spanning the same time period. As discussed previously, climate model simulations predict a decrease in ozone levels in the tropics and their enhancement at higher latitudes. This study is designed to establish a fine parameterisation of UVI modelling in the tropics in order to later couple radiative transfer modelling and a chemistry climate model to obtain precise UVI projections.

Reunion Island is a small tropical island located in the Indian Ocean at a latitude of 20.90° S and a longitude of 55.50° E. This island is very mountainous with a peak at 3070 m a.s.l. and a mean altitude of $\sim$ 600 m a.s.l.. Almost all of the ground measurements were made at Reunion Island University, which is situated in the north of the island at an altitude of 80.0 m and less than 2 km from the coast. The atmosphere in the boundary layer is dominated by the ocean and is often clean with low aerosol concentration. The usual weather follows a typical pattern during the day due to the trade winds: the sky is usually free of clouds at sunrise, but clouds start to appear during the day as the trade winds blow onto the mountain. There is a strong contrast between the east and west sides of the island, because the accumulation of clouds leads to more precipitation on the east coast, while the west coast is mostly dry.

Surface UV measurements show a very high UV index compared to other sites at the same latitude (Lee-Taylor et al., 2010). Aerosol optical thickness shows a mean value of $\sim$ 0.07 at 440 nm, with an occasional maximum at $\sim$ 0.3. These multiple conditions – mountainous, tropical island with low aerosol concentrations – makes Reunion Island an interesting site for studying surface UV radiation. Since the island presents a very high UVI, and the population lives at low to relatively high altitudes, the highest cities being located at about 1.5 km a.s.l., surface UV radiation is a significant health concern. Note that the time zone of the site is UTC + 04:00.

In Sect. 2, we will first present the different data and the radiative transfer model used in this study. As discussed previously, clouds are an important factor of UV variability and, since clouds are not well resolved in the radiative transfer model, we chose to work only on clear-sky UVI modelling here. The data sets used in this study will also be presented.

In Sect. 3, we will address the filtering method used to select only UVI observations for clear-sky conditions with the use of broadband pyranometer global and diffuse solar irradiances and Long et al. (2006) algorithm. A brief comparison will be made with a human observer's report on cloud coverage.

In Sect. 4, we will discuss the radiative transfer model sensitivity to various input parameters. Multiple modelling cases were run using different ozone and aerosol data at the time of the UV measurements and with different input ozone cross sections and solar irradiance spectra at the top of the atmosphere. The impact on the UVI modelled will be analysed.

In Sect. 5, the model will be validated against the clear-sky UVI observations on Reunion Island. We will investigate the model's ability to reproduce diurnal and seasonal variation of UVI, and its ability to reproduce the effect of total ozone column (TO_3) variation on UVI. Lastly we will discuss the results and draw some conclusions. A glossary of all abbreviated terms is available as a Supplement.

2 Data sets

The multiple types of measurements used in this study, as input for the radiative transfer model or as reference to validate the model output, are summarised in Table 1.

UVI measurements were taken with a Bentham DTMc300 spectroradiometer affiliated with NDACC. This spectroradiometer is composed of two monochromators and scans the wavelength range of 280–450 nm. According to Brogniez et al. (2016), Bentham DTMc300 UVI measurements have an expected uncertainty of about 5 % for a coverage factor of 2. Recalibration is made every 3 to 4 months with a 150 W

Table 1. Data sets.

Data	Instrument	Location	Frequency	Contact (PI)	Affiliation
UV index (UV spectrum integrated following McKinlay and Diffey, 1987)	Bentham DM300	Saint-Denis Réunion Island University	dt = 15 min dw = 0.5 nm [280–450 nm]	C. Brogniez	LOA[a] (Lille, France)
Aerosol optical thickness at 340 nm (AOT) Single-scattering albedo at 438 nm (SSA) Ångström exponent at 340–440 nm (α)	Cimel Sunphotometer	Saint-Denis Réunion Island University	Daily mean	P. Goloub	LOA[a] (Lille, France)
Cloud	Observer report	Saint-Denis Gillot	dt = 1 h	F. Bonnardot	MF[b] (Saint-Denis)
Global and diffuse total irradiance	SPN1 Shaded Pyranometer	Saint-Denis Réunion Island University	dt = 1 min	B. Morel P. Jeanty	LE2P[c] (Saint-Denis)
Total ozone column (TO_3)	SAOZ	Saint-Denis Réunion Island University	Daily	A. Pazmino T.Portafaix	LATMOS (Paris, France) LACy[e] (Saint-Denis)
	SBUV2	Satellite	Daily overpass	Richard McPeters	NASA
	OMI-DOAS	Satellite	Daily overpass	P. Veefkind	KNMI (Netherlands)
Total nitrogen dioxide column (TNO_2)	SAOZ	Saint-Denis Réunion Island University	Daily	A. Pazmino T.Portafaix	LATMOS[d] (Paris, France) LACy[e] (Saint-Denis)
Ozone and temperature profiles	Ozone sonde	Saint-Denis Réunion Island University	Weekly	F. Posny	LACy[e] (Saint-Denis) Réunion Island University
	MLS	Satellite	Daily overpass	L. Froidevaux	NASA-JPL

[a] LOA: Laboratoire d'Optique Atmosphérique. [b] MF: Météo France. [c] LE2P: Laboratoire d'Energétique, d'Electronique et Procédé. [d] LATMOS: Laboratoire Atmosphères, Milieux, Observations Spatiales. [e] LACy: Laboratoire de l'Atmosphère et des Cyclones.

lamp and a 1000 W quartz tungsten halogen lamp traceable to National Institute of Standards and Technology. In this study, we used the standard erythemal action spectrum published by the International Commission on Illumination to calculate erythemal-weighted UV (Commission Internationale de l'Eclairage, 1998). Simulation experiments under clear-sky conditions were conducted over the time period covered by SUR measurements, i.e. from 2009 to 2015. The data used in this study for modelling are described below.

TO_3 measurements are as follows:

- ground-based measurements from the SAOZ (Système d'Analyse par Observation Zenithal) (Pommereau and Goutail, 1988) UV-visible spectrometer collocated with the Bentham,
- satellite measurements from OMI (OMTO3 product) and SBUV (Bhartia and Wellemeyer, 2002).

Extraterrestrial solar spectra (ETS) were obtained from

- Chance and Kurucz (2010),
- Dobber et al. (2008).

Several data sets are available of ozone cross sections (O3XS) absorption:

- Malicet et al. (1995) and Brion et al. (1998) (BDM) works are currently used for SBUV instruments:
  - 280–345 nm at 295, 243, 228 and 218 K from Malicet et al. (1995).
  - 345–450 nm at 195 K from Brion et al. (1998).
- Bass and Paur (1985) (BP) are used currently for OMTO3.
- Gorshelev et al. (2014) and Serdyuchenko et al. (2014) obtained high spectral resolution ozone absorption cross sections (called SER hereafter) from a combination of Fourier transform and Echelle spectrometers. Measurements, data analysis and comparisons are presented in the first paper (Gorshelev et al., 2014), and temperature dependence is investigated throughout the second paper (Serdyuchenko et al., 2014).

Orphal et al. (2016) published a recent report on the evaluation of different absorption cross sections of ozone. They

found that BP data should no longer be used for retrieval of atmosphere ozone measurements. Either BDM or SER should be used in ground-based or satellite retrieval. These findings led us to choose BDM and SER O3XS in our current study.

Ozone and temperature profiles came from radiosoundings that have been taken weekly on Reunion Island since 1993, and from MLS satellite measurements (Froidevaux et al., 2008). Nitrogen dioxide measurements were obtained with the SAOZ spectrometer. Aerosol measurements were derived from Cimel sun photometer measurements between 2009 and 2016. Cloud observer reports were made on Reunion Island every hour at about 10 km north of the UVI measurements, while global and diffuse total irradiance were measured every minute at the same location as the UVI measurements.

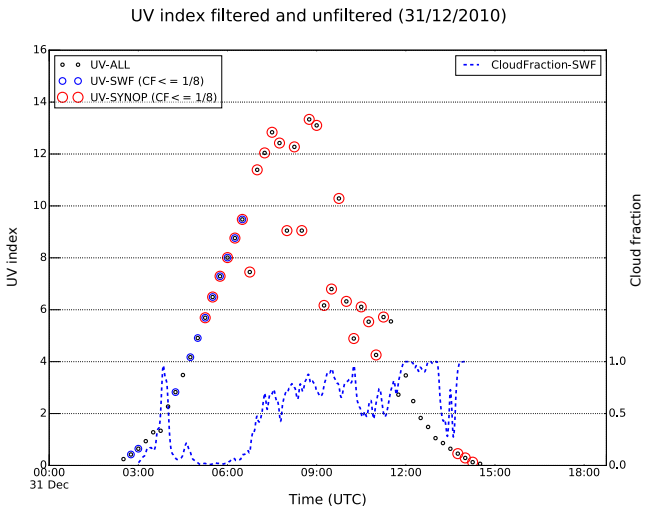

Figure 1. Daily UV index at Reunion Island on 31 December 2010; for UV-ALL Bentham measurements in black circles, UV-SWF: UV data filtered with CF-SWF in blue circles, UV-SYNOP: UV data filtered with CF-SYNOP in red circles. Cloud fraction (CF-SWF) is also represented by the blue dashed line.

3 Clear-sky filtering

Clouds are known to play an important role in surface UV variability (Bais et al., 1993; Calbó et al., 2005 and Mayer et al., 1998). As mentioned previously, this study was limited to clear-sky UV observations and simulations. In order to filter out cloudy conditions, two different methods were used. The first, commonly used one was based on synoptic observer reports (SYNOP) made at a Météo France weather station located about 10 km from the UV measurements site. The observer reports follow WMO guidelines for cloud observations (http://worldweather.wmo.int/oktas). Sky observations are made every hour and are quantified on a scale in oktas from 0 (clear-sky) to 8 (totally overcast sky). We kept only UV measurements made for cloudiness ≤ 1 okta. Since the UV measurements are made every 15 min and sky observer reports are hourly, we interpolated these observations every 15 min. The effect of interpolation is taken into consideration and analysed below. The second method used Long and Ackerman (2000) and Long et al. (2006) algorithms. As input for this algorithm we used 1 min data of global and diffuse total irradiances measured at the same location as the UV measurements, with a SPN1 shaded pyranometer. These algorithms performed multiple tests on the global, diffuse and direct irradiance in order to identify periods of clear skies. They have been validated against a whole sky imager, lidar data and observer reports (Long et al., 2006).

In order to compare the two methods, we tried multiple thresholds of the cloud fraction for the Cloud Observer Report (CF-SYNOP) and cloud fraction obtained with the Long et al. (2006) algorithm, called CF-SWF hereafter. We considered that clear-sky conditions prevailed when the cloud fraction was less than or equal to the CF-SYNOP or CF-SWF thresholds. From these we obtained UVI filtered data, called UV-SYNOP and UV-SWF hereafter.

We investigated numerous days and found CF-SWF to be more responsive and consistent with the UVI measurements. An example of a typical day with varying cloud fractions is represented in Fig. 1. UVI corresponding to all-sky conditions (UV-ALL) are marked in black circles. The blue circles represent UV-SWF and the red ones UV-SYNOP. CF-SWF is also represented by the blue dashed line. A clear-sky day would produce a UVI diurnal cycle resembling a Gaussian-shaped function centred on the solar noon, while moderate to high cloud fractions would generally reduce UVI. In some cases, broken cloud conditions may increase UVI by 20 % relative to clear-sky conditions (Cede et al., 2002). Early in the day, at about 04:00 UTC, both UV-SYNOP and UV-SWF are absent, as no clear-sky conditions are detected: cloud fraction at that time is quite high and impacts the UVI slightly. At around 09:00 UTC we clearly see the impact of a rising CF on UV-ALL, which rapidly decreases. UV-SWF is absent, but CF-SYNOP still labels UV-ALL measurements (UV-SYNOP) as clear-sky while they are clearly not. This example, among many others, made us decide to use only UV-SWF for the UVI clear-sky measurements in all further work.

We then investigated the daily and monthly densities of UVI measurements. In Fig. 2a, average UVI data distribution through the day represents UV-ALL (green bars) and UV-SWF (blue bars), along with the mean CF-SWF (black dashed line). We can see that UV-ALL is equally distributed through the day, since UVI measurements are made every day at 15 min intervals. In contrast, for clear-sky data UV-SWF, there are more measurements available in the morning than in the afternoon, which is anti-correlated with the mean climatological CF-SWF. As clouds tend to form during the day, clear-sky UV measurements are less frequent in

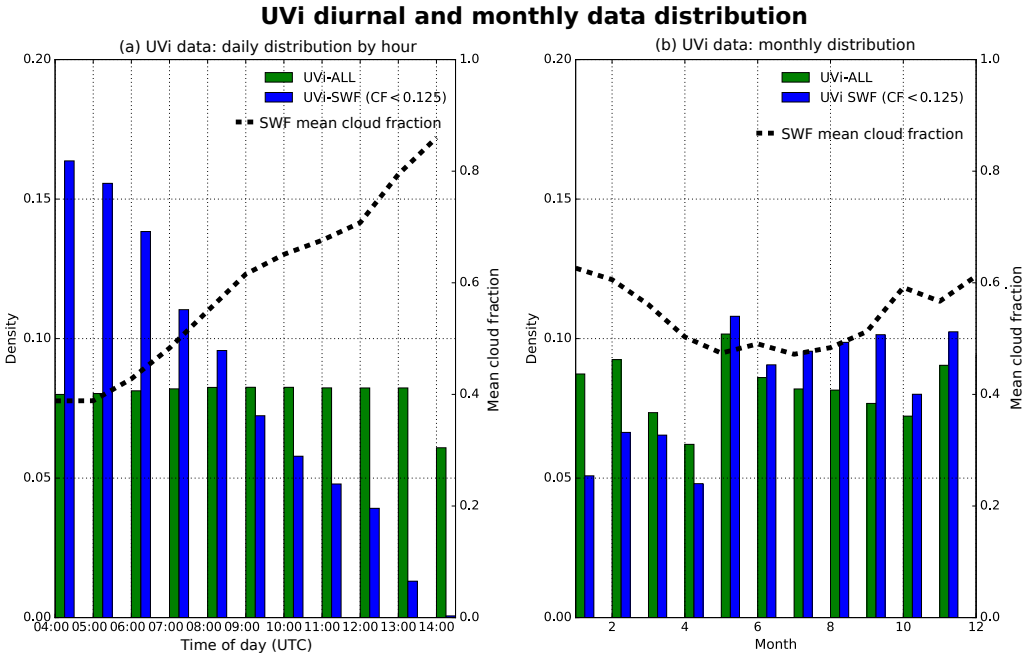

Figure 2. UVI data distribution and cloud fraction for 1 h bins. UVI-ALL is in green, UVI-SWF is in blue, cloud fraction is indicated by the dotted line.

the afternoon. In Fig. 2b, which represents UVI data distribution during the year, we see that UV-ALL are not equally distributed. There are fewer UV-ALL data for the first 4 months, especially during March and April, due to a few failures and technical maintenance of the Bentham spectroradiometer during the 6 years analysed here. We then see a seasonal variation of the availability of clear-sky UVI measurements. During the austral summer, there is an increasing mean cloud fraction and therefore fewer clear-sky measurements. Since the solar zenith angle and total ozone column also follow a diurnal and annual variability, respectively, the uneven clear-sky UVI distribution through the day or through the year will induce a statistical bias on the following comparisons. The threshold chosen for the rest of the study is one-eighth. There was 85 412 measurements. After clear-sky filtering only 16 390 remained.

4 UV modelling

4.1 Radiative transfer model

For UVI modelling, we used the Tropospheric Ultraviolet Visible (TUV) radiative transfer model version 5.3 (Madronich, 1993). TUV is available with two different radiative transfer schemes. We used the pseudo-spherical 8-stream discrete ordinates (psndo.f) (Stamnes et al., 1988) method to solve the radiative transfer equation. The computation time is higher than with the generalised 2-stream method (Toon et al., 1989), also available in TUV, but psndo.f is more accurate (Petropavlovskikh and Brasseur, 1995). N-stream discrete ordinates schemes use analytical treatment before computation. The radiative transfer equation is decomposed into a $2N$ differential equation. Then, with appropriate boundary conditions, the system is numerically solved for each layer of the atmosphere. No approximation is made on the vertical inhomogeneity of the atmosphere or on the phase function. Without computational time requirement, these schemes can have high levels of accuracy. On the other hand, 2-stream methods assume an irradiance independent of the azimuth angle and divide it into upward and downward components. These approximations induce errors, specifically in the lower troposphere and on the diffuse part of the irradiance.

The following parameters were modified in the model in order to reproduce the UVI measurements and site-specific climatology:

- extraterrestrial spectrum (ETS),
- solar zenith angle (SZA),
- total ozone column amount (TO_3),
- total nitrogen dioxide (TNO_2),
- ozone profile (OP),
- temperature profile (TP),
- aerosol optical thickness (AOT) at 340 nm,

- aerosol Ångström exponent (α) between 340 and 440 nm,
- single-scattering albedo (SSA) (Takemura et al., 2002 and Lacagnina et al., 2015; see below for more details),
- ground surface albedo (alb),
- altitude (z).

Due to the lack of reliable data, total column sulfur dioxide (TSO_2) was set to zero, which could induce a modelling error during a volcanic eruption. Between 2009 and 2015, there were a few volcanic eruptions from the Piton de la Fournaise, which is located on the opposite coast of Reunion Island to the site where the UVI measurements were taken. Unfortunately there are no TSO_2 data available for this period. Following McPeters and Labow (2012), a monthly climatology of ozone and temperature profile was derived from ozone soundings and MLS satellite measurements. Single-scattering albedo from the Cimel sun photometer was not usable, as Dubovik et al. (2000) showed that SSA has a large uncertainty if the AOT is lower than 0.3, which was almost always the case here. As proposed by Lacagnina et al. (2015) and Takemura et al. (2002), a fixed SSA of 0.95 was set. The errors due to the use of a standard SSA were not investigated here and should be investigated in the future (Correa et al., 2013).

Following Koelemeijer et al. (2003), surface albedo was taken to be constant at 0.08. According to Koepke et al. (1998), the UVI modelling error is about 5 % for a coverage factor of 2.

4.2 Influence of input parameters

To study the impact of various inputs on surface UV calculations, we tested multiple inputs from a baseline configuration (Table 2). Then different RTUV (Reunion Tropospheric Ultraviolet) cases were run with only one parameter varying in each (Table 3).

4.2.1 Earth–Sun distance and extra-terrestrial spectrum

In order to take into account the varying Earth–Sun distance (ESD, in astronomical unit), a time dependent coefficient (ESF) is used in TUV: $\mathrm{ESF}(t) = 1/\mathrm{ESD}^2$. The new extraterrestrial spectrum ET′, which is the spectrum at the top of the atmosphere corrected for any instant of time (it) is then (1):

$$\mathrm{ET}' = \mathrm{ESF(it)} \times \mathrm{ET}. \quad (1)$$

For convenience, we will now refer to the corrected extraterrestrial spectrum simply as ET. The ESD correction is done when RTUV is used for time series studies but, in order to study the sensitivity to the ET spectrum (or to the O3XS later in Sect. 4.2.2), we chose to run TUV in an idealised state (i-RTUV), with constant Earth–Sun distance, total ozone column varying from 250 to 350 DU, solar zenith angle varying from 0 to 60° and mean values of aerosol representing the entire study period (see Table 3).

Table 2. Baseline configuration of the TUV model.

Parameter	
Period	2009–2016
Latitude	−20.90
Longitude	55.50
Temporal resolution (dt)	15 min
Vertical scale	0–80 km
Vertical resolution (dz)	1 km
Wavelength	280–450 nm
Wavelength resolution (dw)	0.5 nm
Albedo	Koelemeijer et al. (2003)
TNO_2	SAOZ
TSO_2	0
Cloud fraction	0
OP	McPeters and Labow (2012)
TP	McPeters and Labow (2012)
SSA	0.95
Aerosol profile	Elterman (1968)

Since we want to understand the sensitivity to the ET spectrum, i-RTUV was run with the Dobber et al. (2008) or Chance and Kurucz (2010) ET spectrum. From there we took UVI output and defined the UVI relative difference (RD) between these two cases as

$$\mathrm{RD}[\%] = 200 \times \frac{\mathrm{UVI_{dobber}} - \mathrm{UVI_{chance}}}{\mathrm{UVI_{dobber}} + \mathrm{UVI_{chance}}}. \quad (2)$$

RD on the surface UVI modelled between the two ET spectra for the SZA and TO_3 studied is represented in a monthly climatological OP and TP in Fig. 4a for January and in Fig. 4b for October. The highest RD appears to occur for low SZA and low TO_3, at about 5 % for January and about 4 % for October. Minima of RD are for high SZA and high TO_3, at about 3 and 2 % for January and October, respectively. At fixed TO_3, when SZA increases, the path length travelled by the radiation crossing the atmosphere is longer and other processes, such as Rayleigh scattering, have more impact on the surface UVI modelled than different ET spectra. At fixed SZA, when TO_3 increases, the RD decreases, or when ozone molecular absorption increases the differences in the ET spectra are less important.

During the month of October, OP shifts from the annual mean (Fig. 3). There is an increase in tropospheric ozone through the arrival of emissions due to biomass burning over the western part of the Indian Ocean zone (Baldy et al., 1996). The absorption effectiveness of tropospheric ozone relative to stratospheric ozone depends on SZA (Brühl and Crutzen, 1989). This is why there is a small difference (about 1 %) between January and October. This difference is only due to the shift in ozone and temperature profiles.

Table 3. Case configurations.

Case	TO_3	Aerosols	ETS	O_3 XS	ESD
RTUV01	SAOZ	Cimel daily	Dobber et al. (2008)	SER	f(t)
RTUV02	OMI	Cimel daily	Dobber et al. (2008)	SER	f(t)
RTUV03	SBUV	Cimel daily	Dobber et al. (2008)	SER	f(t)
RTUV04	SAOZ	Cimel monthly Clim	Dobber et al. (2008)	SER	f(t)
RTUV05	SAOZ	Cimel daily	Chance and Kurucz (2010)	SER	f(t)
RTUV06	SAOZ	Cimel daily	Dobber et al. (2008)	BDM	f(t)
RTUV07	SAOZ	AOT: 0.05	Dobber et al. (2008)	SER	
		SSA: 0.95			esfact = 1
		α: 0.90			
i-RTUV	250–345 DU	AOT: 0.05	Dobber et al. (2008)	SER	Constant
		SSA: 0.95	or	or	esfact = 1
		α: 0.90	Chance and Kurucz (2010)	BDM	SZA = [0,60]°

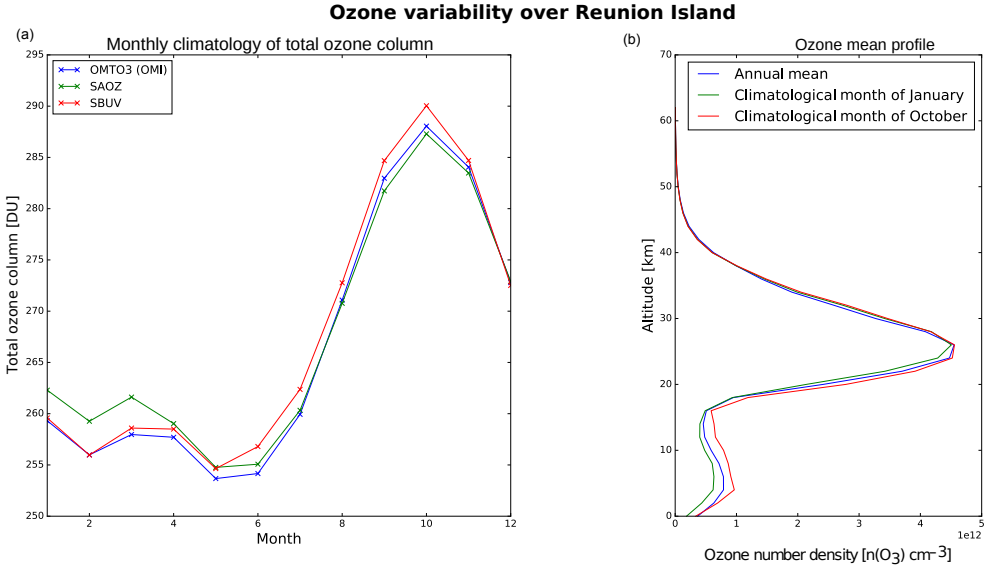

Figure 3. Ozone variability over Reunion Island. **(a)** Monthly climatology of total ozone column for three data sets (OMI in blue, SAOZ in green and SBUV in red). **(b)** Mean ozone profile from McPeters and Labow (2012) climatology. Annual mean in blue, January in green and October in red.

In Fig. 4c, the monthly mean of UVI RD between RTUV05 and RTUV01 is represented by a dashed blue line. These two RTUV cases have the same configuration except for the ET spectrum. The sign of the RD here is coherent with Eq. (2), i.e. RTUV05 (Chance ET) minus RTUV01 (Dobber ET). The monthly mean of RD between these cases oscillates between 2.7 and 3.4 %, these values being of the same of order as the i-RTUV cases. The oscillation observed here is anti-correlated with the maximum of SZA at solar noon at the site studied.

To conclude, UVI dependency on the ET spectra is higher at low SZA and low TO_3, which are also the conditions where we find the maximum of UVI, i.e where the health risk is highest. While the RD is dependent on SZA and TO_3 (at about 3.0 %), OP and TP also constitute factors of variability (about 1 %). RD is modulated through the year with the variation of SZA. Finally, Chance's spectrum impact on the surface UVI modelled will be an increase of about 3.0 % with respect to Dobber's.

4.2.2 Ozone cross sections

Following these studies we investigated the impact on simulated UV irradiance modelled with different absorption cross sections of ozone (O3XS). As mentioned previously we used BDM and SER and defined the relative difference between the two modelling cases as

$$\mathrm{RD}[\%] = 200 \times \frac{x_{\mathrm{BDM}} - x_{\mathrm{SER}}}{x_{\mathrm{BDM}} + x_{\mathrm{SER}}}. \quad (3)$$

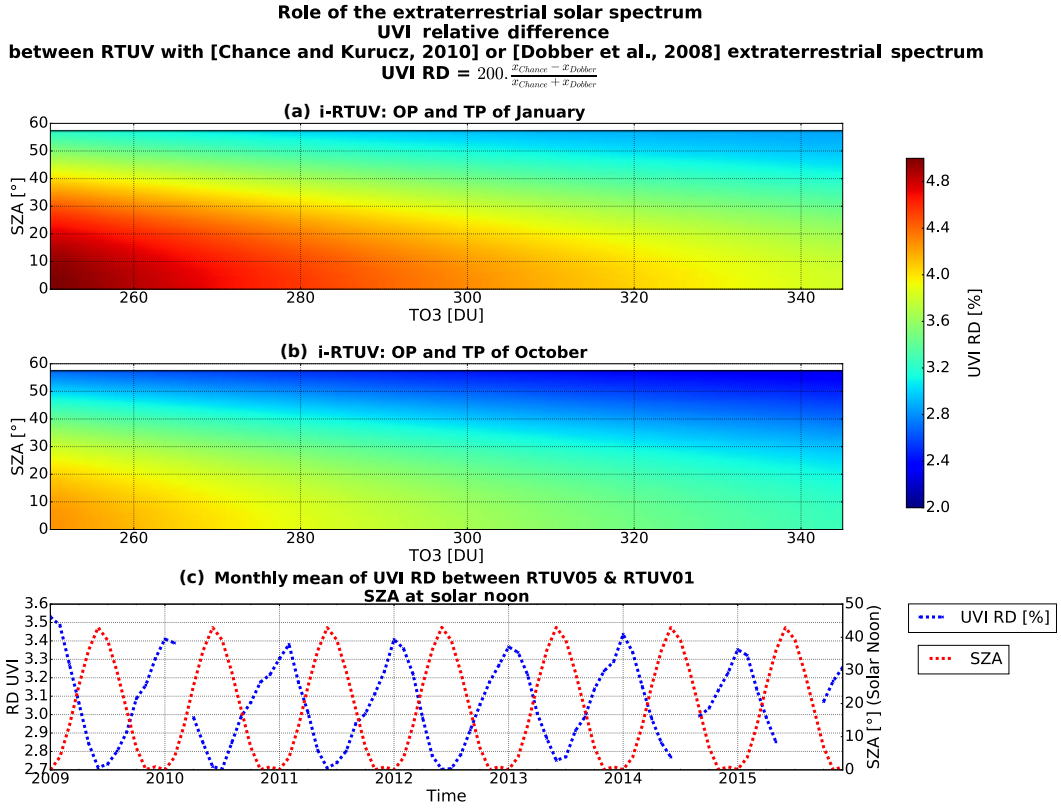

Figure 4. **(a)** UVI relative difference between two idealised runs with different ET spectra for a varying TO_3 and SZA for a climatological OP and TP of January. **(b)** Same as panel **(a)** but for OP and TP of October. **(c)** Monthly mean of UVI RD between RTUV05 and RTUV01 (blue dashed line). Monthly mean of SZA at solar noon. (red dashed line).

Figure 5a represents the UVI RD using two different O3XS (Eq. 3) in an idealised run (i-RTUV) for October OP and TP climatologies. Here, RD ranges from 2.4 to 2.9 %. We observe the same variability as for the ET sensitivity: the highest values of RD correspond to low SZA and low TO_3, and as either SZA or TO_3 increases, UVI RD will decrease. Figure 5b shows the role of the varying Earth–Sun distance by using the corresponding RTUV cases (RTUV06 with BDM and RTUV01 with SER), which differ only by O3XS. There is also a yearly UVI RD oscillation anti-correlated with the maxima of SZA at solar noon. The mean RD is about 2.7 %, which is consistent with the i-RTUV case. The oscillation around the annual mean is smaller here than for the ET spectra (about 0.5 %) but so is the mean RD.

To summarise O3XS for this studied site, using SER O3XS instead of BDM O3XS increases the mean surface UVI by about 2.7 %. This UVI RD is modulated by the SZA, TO_3, OP and TP.

4.2.3 Total ozone column

Three different TO_3 data sets covering the period 2009 to 2016 in RTUV01 (SAOZ), RTUV02 (OMTO3) and RTUV03 (SBUV) were investigated. In contrast to the simulations in the idealised state, these simulations were conducted with varying Earth–Sun distance. The relative difference distributions for TO_3 and UVI are represented in Fig. 6 with 1 % bins. Mean RD between TO_3 data sets is smaller than 0.3 % with a standard deviation of about 2 %. The impact on the surface UVI modelled is slightly higher. There is a small mean relative difference of $\approx 0.1 \pm 2.3$ % between SBUV and OMTO3, 0.4 ± 2.0 % between SAOZ and OMTO3 and -0.3 ± 1.8 % between SAOZ and SBUV.

Since TO_3 and surface UVI are anti-correlated, a positive RD in TO_3 will lead to a negative RD on UVI and vice versa. This is expressed by the opposite sign of the mean RD between TO_3 and UVI and by the RD distribution. If the distribution of RD of TO_3 tends to shift towards positive values, the distribution of UVI RD will shift towards negative values.

4.2.4 Aerosol climatology and observations

Aerosol concentrations are usually very low in this region except during a specific period of biomass burning or volcanic eruption. Here the objective is to evaluate the impact of the aerosol variability on UVI modelling.

Figure 7a, b and c represent the monthly climatological values of AOT, SSA and Ångström exponent provided by

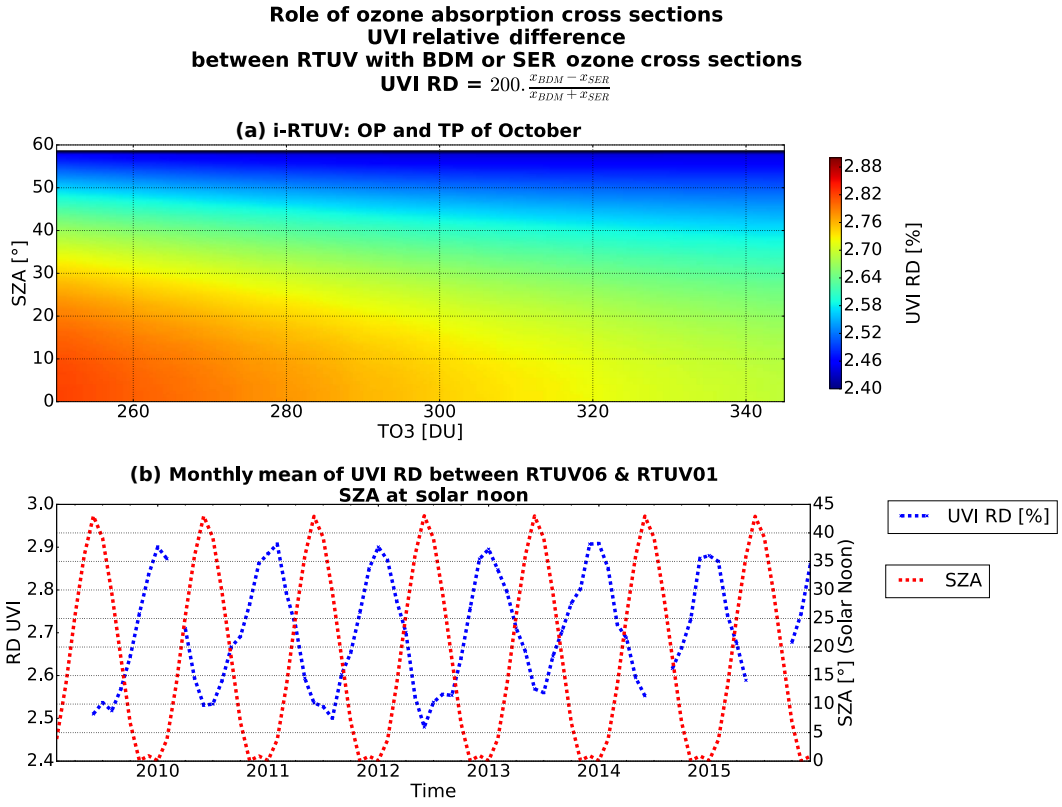

Figure 5. (a) UVI relative difference between two idealised runs with different O3XS for a varying TO_3 and SZA and for climatological OP and TP of October. **(b)** Monthly mean of UVI RD between RTUV06 and RTUV01 (blue dashed line). Monthly mean of SZA at solar noon (red dashed line).

a Cimel instrument. Aerosol optical thicknesses are usually quite low. There is a peak centred around October. It coincides with the arrival of biomass burning emissions over the western part of the Indian Ocean zone (Baldy et al., 1996). In Fig. 7b, the monthly climatologies of SSA (at 438 nm) derived from Cimel measurements are represented. These values are very uncertain as mentioned previously. Ångström exponent represents 340–440 nm and describes the spectral dependence of the AOT.

As aerosol input for UVI modelling, two data sets were used in this study, one being a monthly climatology derived from the Cimel sun photometer measurements from 2009 to 2016 and hereafter called Cimel Clim, and the other being the daily mean derived from the same instrument and hereafter called Cimel daily. RTUV01 was run with Cimel daily and RTUV 04 with Cimel Clim (see Table 3). We define the AOT anomaly as the difference between AOT daily mean and monthly climatology:

$$\mathrm{AOTANOM} = \mathrm{AOT}_{\mathrm{Cimeldaily}} - \mathrm{AOT}_{\mathrm{CimelClim}}. \quad (4)$$

Figure 7d represents the aerosol daily anomaly for the entire study period. We can observe few sharp peaks of a 0.25 AOT anomaly and several decreases to about a 0.1 AOT anomaly. The maximum anomaly usually appears at the end of the year. Most of these anomalies are due to biomass burning emissions. Figure 7e shows UVI RD between RTUV04 and RTUV01. The succession of AOT anomalies has a direct impact on surface UVI; for the 0.25 increase in AOT, during the end of 2010, there is a $\approx 30\,\%$ relative difference between the two surface UVI modelled. This is better observed on Fig. 7f and g, which represent the monthly distribution of positive AOT anomalies and negative UVI relative difference split into three categories. Quantitatively more AOT anomalies (more than 0.15 AOT daily anomalies) are centred around October, which leads to higher values of UVI relative difference.

To summarise the aerosol findings, even though the mean relative differences in surface UVI for the two cases are very low for the entire studied period ($-0.40\,\%$), there is still a punctual effect where surface UVI could be overestimated by $\sim 30\,\%$ when using aerosol climatology.

5 Model validation

In this section, we compare observations made only in clear-sky conditions against the different RTUV modelling cases (Table 3).

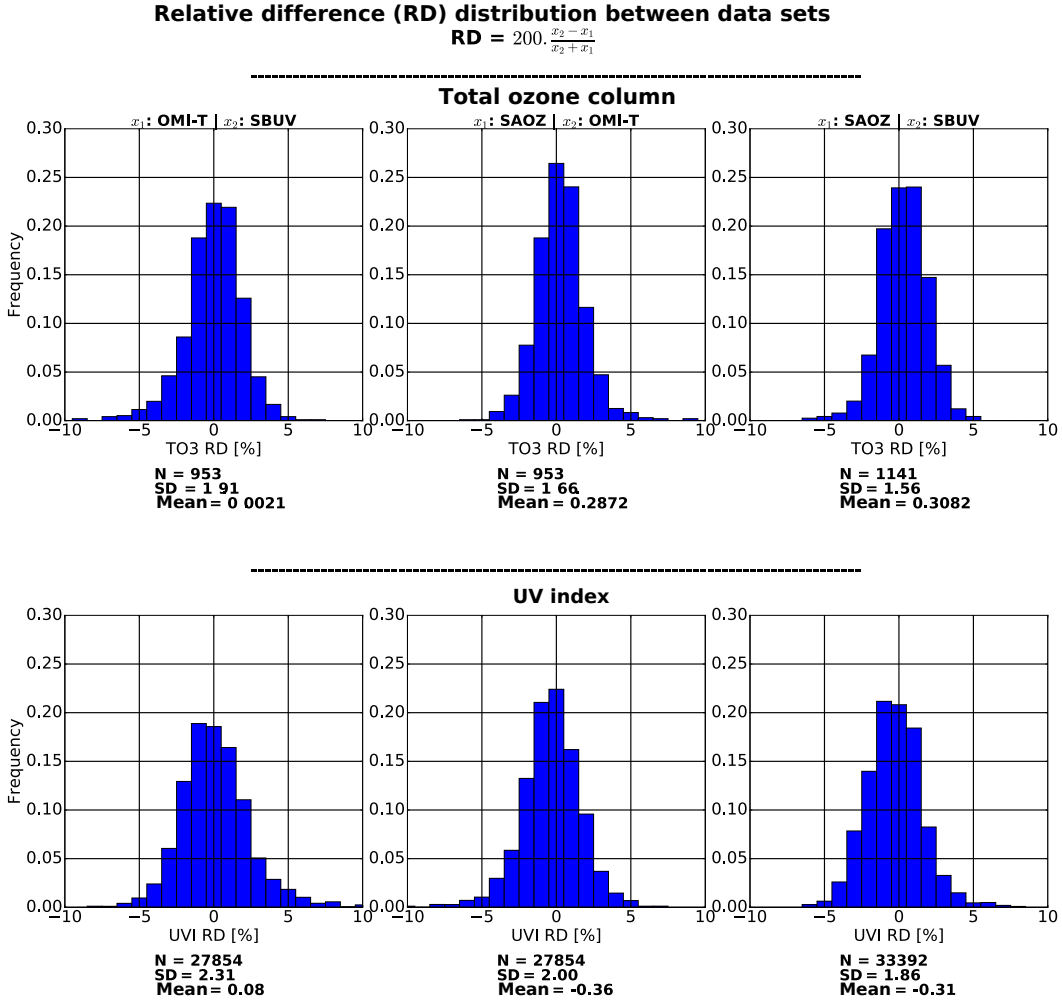

Figure 6. Distribution of relative difference (%) between different TO_3 data sets and between the corresponding surface UVI modelled at all SZA.

5.1 Radiative amplification factor

To study the sensitivity of the modelling output to TO_3, we need to understand the variability of UVI and ozone. The scaling function between UVI and ozone is commonly described as the radiative amplification factor (RAF). Following Madronich (1993), we define the RAF as a power law:

$$\frac{\mathrm{UVI}_{t_1}}{\mathrm{UVI}_{t_2}} = \left(\frac{\mathrm{TO_3}_{t_1}}{\mathrm{TO_3}_{t_2}}\right)^{-\mathrm{RAF_P}} \tag{5}$$

$$\mathrm{RAF_P} = \ln\left(\frac{\mathrm{UVI}_{t_1}}{\mathrm{UVI}_{t_2}}\right) / \ln\left(\frac{\mathrm{TO_3}_{t_2}}{\mathrm{TO_3}_{t_1}}\right). \tag{6}$$

From there we can take every total ozone column measurement at a specific date t and the corresponding UVI and compute ratio.

If we derive the power law we can obtain a linear form of the RAF (Booth and Madronich, 1994):

$$\mathrm{RAF_L} = -\frac{\Delta\mathrm{UVI}}{\mathrm{UVI}_{t_1}} \Big/ \frac{\Delta\mathrm{TO_3}}{\mathrm{TO_3}_{t_1}}. \tag{7}$$

Since the derivative is local, only a small percent change should be used, here we choose to select a percent change smaller than 10 %. We proceed by considering every total ozone column measurement at a specific date t and the corresponding UVI. We then compute the relative difference for a specific SZA interval between all pairs of UVI and TO_3, such as at two dates $t1$ and $t2$:

$$\frac{\Delta\mathrm{UVI}}{\mathrm{UVI}_{t_1}} = \frac{\mathrm{UVI}_{t_1} - \mathrm{UVI}_{t_2}}{\mathrm{UVI}_{t_1}} \tag{8}$$

$$\frac{\Delta\mathrm{TO_3}}{\mathrm{TO_3}_{t_1}} = \frac{\mathrm{TO_3}_{t_1} - \mathrm{TO_3}_{t_2}}{\mathrm{TO_3}_{t_1}}. \tag{9}$$

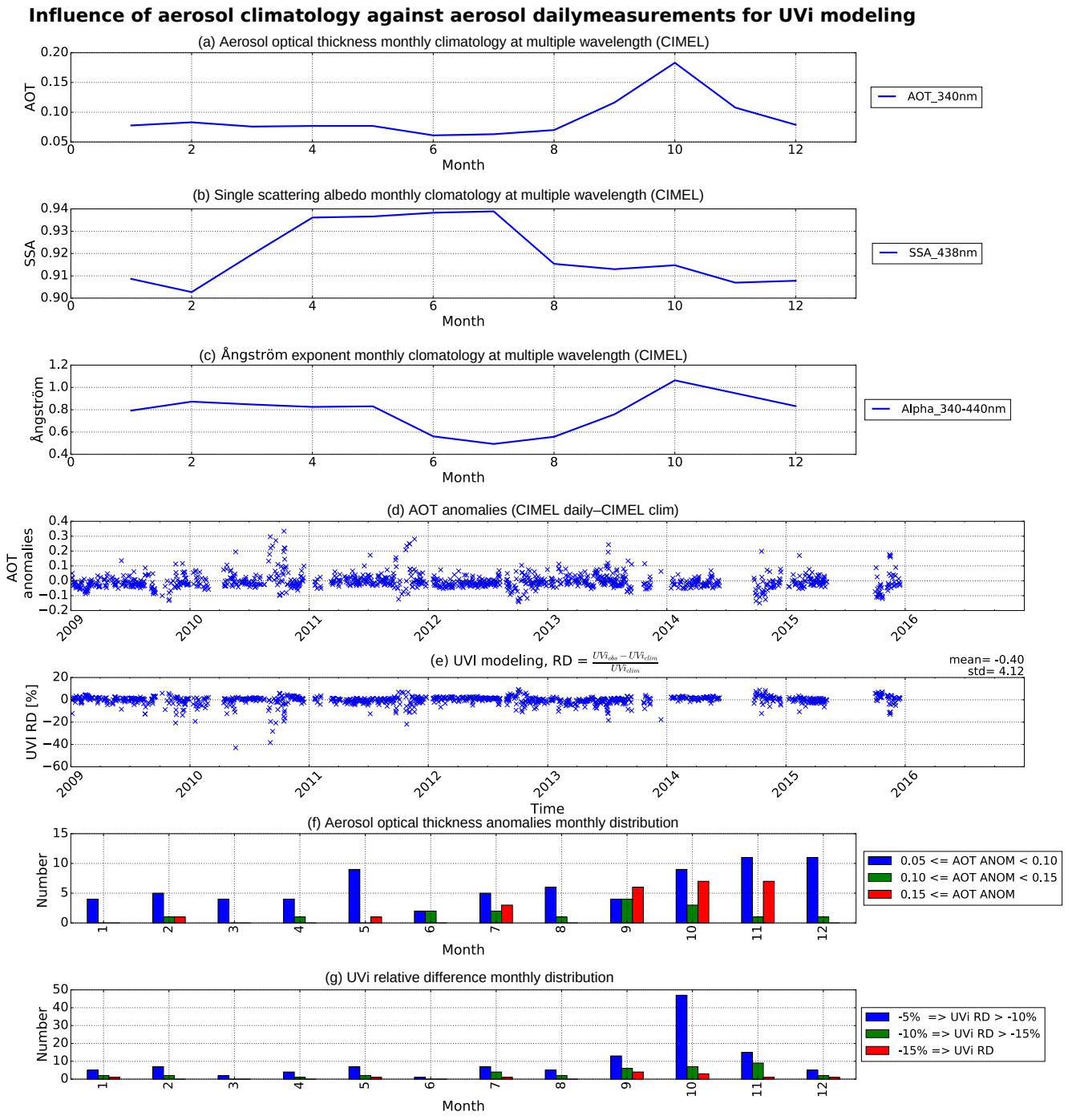

Figure 7. Impact of aerosols on UVI modelling. **(a)** AOT monthly climatology. **(b)** SSA monthly climatology. **(c)** Ångström exponent monthly climatology. **(d)** AOT anomalies during the study period. **(e)** UVI relative difference between a run with climatological aerosols and daily aerosols. **(f)** AOT anomalies distribution. **(g)** UVI relative difference monthly distribution.

In previous works, Booth and Madronich (1994) found a RAF_L of 1.1 from broadband measurements in Antarctica. More recently, from a theoretical point of view, Herman (2010) found a RAF_P of 1.25 at low SZA, decreasing to 1.1 at higher SZA. These values correspond to a mid-latitude profile. Bodhaine et al. (1997) analysed 1 year of UV measurements at Mauna Loa, Hawaii and found RAF_P values between about 1.3 at a SZA of 15° and 0.6 at 85° SZA. At a SZA of 45°, while Bodhaine et al. (1997) found a

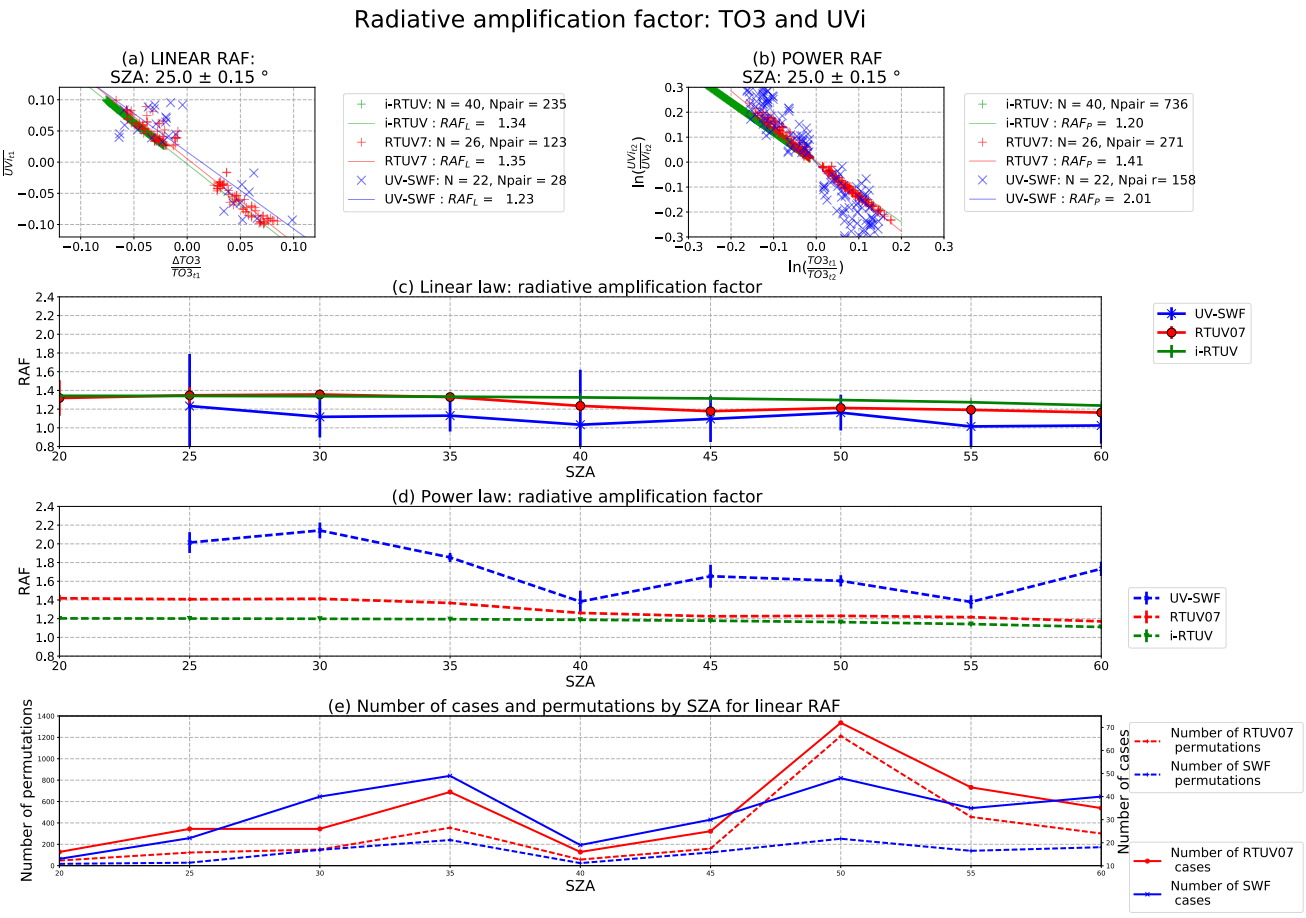

Figure 8. Radiative amplification factor. **(a)** $\Delta UV/UV$ versus $\Delta TO_3 / TO_3$ for UV-SWF (blue crosses), RTUV07 (red crosses) and i-RTUV (green crosses). Linear fitted functions are in coloured curves of corresponding colours. **(b)** Same as panel **(a)** but for a power-law fit between $\ln(UV/UV_{t1})$ and $\ln(O3/O3_{t1})$. **(c, d)** Linear and power RAFs deduced from the previous fit for a varying SZA with a 2σ dispersion bar. **(e)** Number of permutations (N_{pair}) and number of cases (N) available in comparison to SZA for the linear RAF.

RAF_P of 1.38 ± 0.20, McKenzie et al. (1991) found a RAF_P of 1.25 ± 0.20 at Lauder, New Zealand (45° S).

Here, both RAFs (linear and power) are calculated for an ideal modelling case (i-RTUV) with SER O3XS and Dobber ET spectrum, for the observations (UV-SWF) and for a real-condition modelling case (RTUV07) where we fixed every parameter except TO_3 and monthly ozone and temperature profiles. Observations are multiplied by the inverse of the ESF to bring them to constant ESD and be more similar with modelling at constant ESD. The first objective is to evaluate the RAF of TO_3 on the UVI for the three cases, to see how they compare to each other and to determine whether RTUV07 is close to the observations (UV-SWF) by being able to reproduce the RAF of TO_3. The second objective is to compare the RAFs found here with those found previously in other studies at other sites.

In Fig. 8a, $\Delta UVI/UVI$ is plotted against $\Delta TO_3 / TO_3$ for a SZA of $25° \pm 0.1°$ for the three cases. The best-fitting curve of each case is obtained from a least squares fitting method, from which RAF_L is also deduced (Booth and Madronich, 1994). This range of SZAs is chosen due to the availability of measurements. Because of the annual variation of the SZA, lower values of SZA occur during the rainy season, when we filter out most of our data. UV-SWF is in blue, RTUV07 in red and i-RTUV in green. In Fig. 8b, the same method is used to retrieve RAF_P (Madronich, 1993). Figure 8c and d represent RAF_L and RAF_P plotted against SZA for the three cases, with a 2σ dispersion bar. Figure 8e represents the number of cases and permutations used for the regression. Even if the number of permutations which are used for computation of the RAFs are high, the number of cases compared with each other are quite low.

For i-RTUV, RAF_P (dashed green line) are at about 1.20 for a SZA of 25° decreasing to 1.11 for a SZA of 60°, RAF_L (solid green line) decreases from 1.34 to 1.23. Between the same SZAs, while RAF_P derived from the clear-sky observations (UV-SWF, dashed blue line) decreases from 2.01 ± 0.11 to 1.73 ± 0.07, RAF_L (solid blue line) de-

creases from 1.23 ± 0.27 to 1.02 ± 0.09. From RTUV07, RAF_P (dashed red line) ranged between 1.40 ± 0.02 and 1.17 ± 0.07. At a SZA of 45° from the observations, the RAF_P obtained was 1.65 ± 0.12. This value is higher than the one that found by Bodhaine et al. (1997), of 1.38 ± 0.20, for a similar site in the tropics.

RAF tends to decrease as SZA increases. When the SZA increases the path travelled through the atmosphere will be longer and other processes, such as Rayleigh scattering, will have a higher impact on the UVI. Since the absorption effectiveness of tropospheric ozone relative to stratospheric ozone depends on SZA (Brühl and Crutzen, 1989), the ozone distribution and the temperature profile have an impact on the RAF value. This is one of the reasons why both RAFs deduced from i-RTUV cases present a smooth line. In i-RTUV, nothing changes except TO_3 and SZA. However, in UV-SWF, variations in aerosols, TNO_2, ESD, OP and TP between $t1$ and $t2$ are naturally included. In RTUV07 only TO_3, SZA, ozone and temperature profiles are not constant. The impact of OP and TP can be appreciated if we look at the difference between RTUV07 and i-RTUV.

RAF_L determined by the observations (UV-SWF) is always lower than i-RTUV, by about 0.2. However, RAF_P determined by the observations (UV-SWF) is higher than the idealised case by about 0.6 at low SZA, between 25 and 35°. It is closer at higher SZA. The result from the observations should be considered carefully. When two cases are compared the relative difference between every other parameters associated with theses cases (such as AOT, TNO_2 and OP) are selected to be smaller than 10 %. Uncertainties are still important for the corresponding TO_3, AOT, TNO_2, OP, TP and clear-sky filtering associated with each UVI measurement. It is difficult to determine whether observations are better represented by a linear law or a power law as dispersion is high and the number of cases are low (Fig. 8e) for both.

5.2 Validation against observed clear-sky UVI

In order to validate UVI modelling for the southern tropics, we compared the output of multiple model cases against UVI clear-sky measurements. Table 4 presents relative difference and standard deviation for the six Reunion Tropospheric Ultraviolet (RTUV) model cases.

We define the relative difference between RTUV and UV-SWF as

$$\mathrm{RD}[\%] = 100 \times \frac{\mathrm{UVI_{RTUV}} - \mathrm{UVI_{OBS}}}{\mathrm{UVI_{OBS}}}. \quad (10)$$

The closest agreement between the measurements and model is found for the RTUV03 case. This corresponds to a configuration with daily aerosol measurements, Dobber ET spectrum, TO_3 from SBUV and SER ozone cross sections. We compared measurements at SZA $\leq 60°$. Of the three sets of ozone total column, the agreement between the measured and modelled UVIs is optimal when SBUV data set is used as input (RTUV03), with a mean relative difference (MRD) of 0.43 ± 5.60 %. It is 0.11 % lower than RTUV02 (OMI) and 0.51 % lower than the run with SAOZ measurements as input (RTUV01). Standard deviations (SDs) are about the same for the five cases, around 5.7 %. RTUV03 obtains the lowest median (MED) at 0.44 %. Nonetheless, some of those results are not significant because they are lower than the uncertainty of the UVI measurements (±5 %).

For different extraterrestrial spectra in RTUV01 (Dobber et al., 2008) and RTUV05 (Chance and Kurucz, 2010), a 3.24 % difference is found between both MRD and MED. The difference is consistent with the one found in Sect. 4.2.1.

The influence of the choice of ozone cross sections on UVI modelled can be analysed with RTUV01 (SER) and RTUV06 (BDM). The first is 3.44 % lower than the second. The difference between the two is higher here than the difference found previously (Sect. 4.2.2) in an idealised run, where only one profile of temperature and one of ozone were used for the sensitivity test. BDM O3XS (Brion et al., 1998 and Malicet et al., 1995) were calibrated for four temperatures, 295, 243, 228 and 218 K, while SER was run with temperatures ranging from 193 to 293 K with a 10 K step. Since UVI is sensitive to the ozone and temperature profiles, different O3XS can induce higher differences in surface UVI than we calculated previously during the sensitive test. This needs to be investigated further, in particular the impact of O3XS and ozone and temperature profiles on the surface UVI.

A linear regression representation and mean relative difference plots versus SZA are given in Fig. 9 for all RTUV cases. On all subplots of Fig. 9a, data corresponding to a daily mean AOT higher than the monthly mean AOT are represented in red. All conditions are in blue. RTUV01 and RTUV04 use different aerosol inputs, RTUV01 was modelled with an aerosol daily mean and RTUV04 used a monthly climatology. The MRD of RTUV01 is lower than that of RTUV04, whereas the opposite is true for the MED. Unlike the mean, the median is insensitive to outliers. In Sect. 4.2.4 it was noted that, even if MRD is very low, there are also singular peaks that can reach up to 30 % MRD. These are the outliers that are taken into account in RTUV04. Close examination of Fig. 9a reveals consistent outliers under the fitted curves for RTUV01, 02, 03, 05 and 06, which correspond to an underestimation of the UVI (due to an overestimation of AOT). For RTUV04, which is the case with monthly climatological values of AOT, there are of course only blue crosses. Bottom outliers on every other RTUV case can be explained by the use of an AOT daily mean. Since the Cimel sun photometer only takes measurements when the sun is directly visible, and we have previously shown a strong presence of clouds, using an AOT monthly climatology can sometimes be better than the daily mean.

The optimised input configuration is RTUV03. The corresponding statistical values are consistent with those found in other studies. Badosa et al. (2007) found a MRD lower than 10 % concerning observations with a similar instrument and

Table 4. RTUV Cases against clear-sky UVI observations.

Parameter	RTUV01	RTUV02	RTUV03	RTUV04	RTUV05	RTUV06
Mean relative difference (%)	0.94	0.54	0.43	1.29	4.18	4.38
Standard deviation	5.60	5.86	5.83	5.32	5.77	5.78
Median of the RD	1.07	0.70	0.44	0.73	4.31	4.51

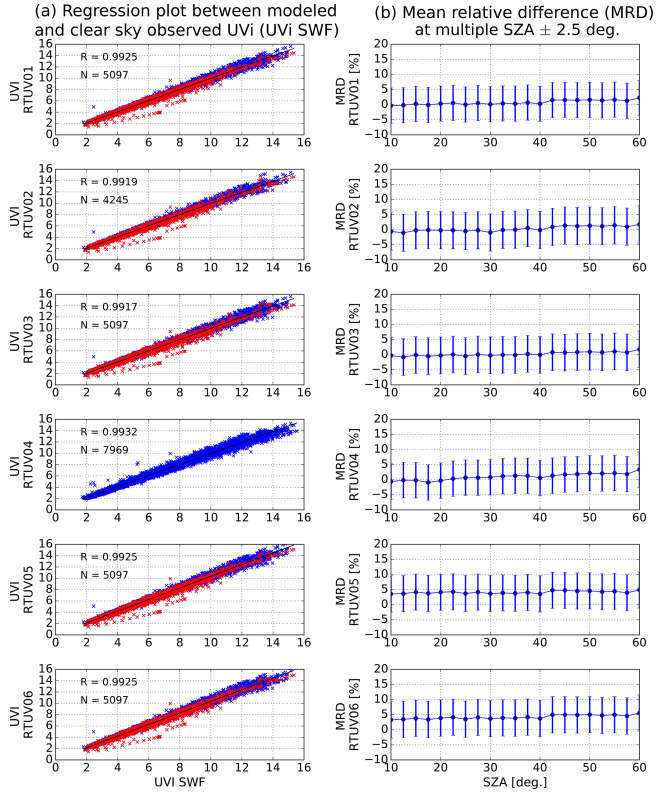

Figure 9. Comparisons of RTUV modelling cases with UVI-SWF observations. **(a)** UVI RTUV against UVI SWF. Linear regression shown with a black line, all RTUV data against UVI SWF are marked with blue crosses, and RTUV data modelled with an AOT higher than the monthly mean AOT are represented in red. **(b)** Mean relative difference for a varying SZA with dispersion bar $\pm 1\ \sigma$ (standard deviation).

filtering techniques at Lauder (45.04° S), Boulder (40.01° N), Mauna Loa (19.53° N) and Melbourne (37.63° S). Mauna Loa can be compared with Reunion Island as both sites are in the tropics and have similar weather conditions. MRD between Badosa et al. (2007) model cases and observations ranged from −1.8 to 3.6 %. In the present study comparable values of MRD were found (ranging from 0.43 to 4.38 %, which is well within the modelling uncertainty of 5 %). The filtering method at Mauna Loa was probably stronger due to the use of a whole sky imager.

Diurnal cycles of RD between RTUV01 and UV-SWF are represented in Fig. 10 for the entire year and for two seasons, austral winter (June, July and August) and austral summer (December, January and February). Since the SAOZ instrument is colocated with the Bentham spectrometer we chose to use RTUV01 for the comparison even if RTUV03 gave better results. RD tends to increase during the day for the whole year and both seasons due to the formation of clouds. The standard deviation is higher in the afternoon during summer due to the strong presence of clouds in this period (see Fig. 2). Since there are fewer clear-sky measurements for this period, the comparison is statistically weaker here, which increased the dispersion. In winter, there is more data available and less filtering (see Fig. 2), so standard deviations are smaller.

In Fig. 11 the diurnal cycle of the UVI seasonal mean and maximum are represented. Consistent results are obtained. Mean non-filtered UVIs are always lower than mean clear-sky values. As mentioned before, the model tends to overestimate clear-sky UVI. Both filtered data sets (UVI-SWF and UVI-SYNOP) are in agreement: UVI-SYNOP diverges from UVI-SWF during the afternoon for the austral summer but, as stated before, SYNOP observer reports are less accurate than SWF cloud fractions. This is probably due to the distance between SYNOP observer reports, which are about 10 km from SWF, and UVI measurements, and the sampling difference: 1 h for SYNOP, 1 min for SWF and 15 min for UV measurements. It would be very interesting to add an all-sky camera to the same site for more accurate indications of cloudiness. Austral summer is usually a very cloudy season in this southern tropical region. A maximum of UVI appears for unfiltered data (green dashed line) with strong values, usually up to 18, around 08:00 UTC (local noon time). This is probably due to UV enhancement by cloud fractional sky cover. This phenomenon has been described before, for example by Calbó et al. (2005) and Jégou et al. (2011), and its quantification in the southern tropics will be the subject of a future study.

6 Conclusions

The physics of radiative transfer is well understood but the modelling of surface UV radiation is still a challenge since multiple parameters need to be taken into account. For clouds, we can simply filter observations and work under clear-sky conditions.

We investigated the sensitivity of clear-sky UV radiation modelling to various input parameters. The impact of dif-

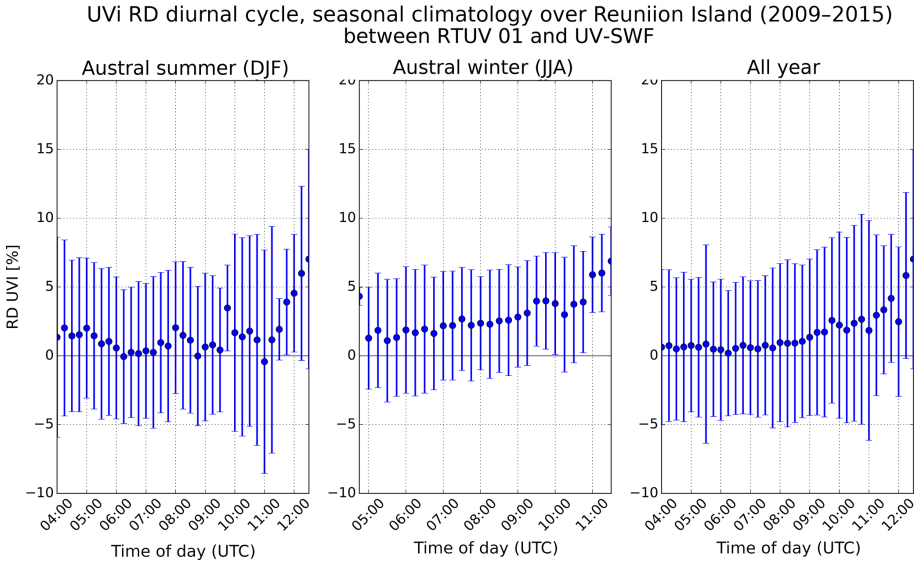

Figure 10. Diurnal cycle of UVI relative difference between RTUV01 and UV-SWF for austral winter, summer and all year. Climatological values of UVI relative differences obtained every 15 min are in blue dots with dispersion bar ($\pm 1\sigma$, standard deviation).

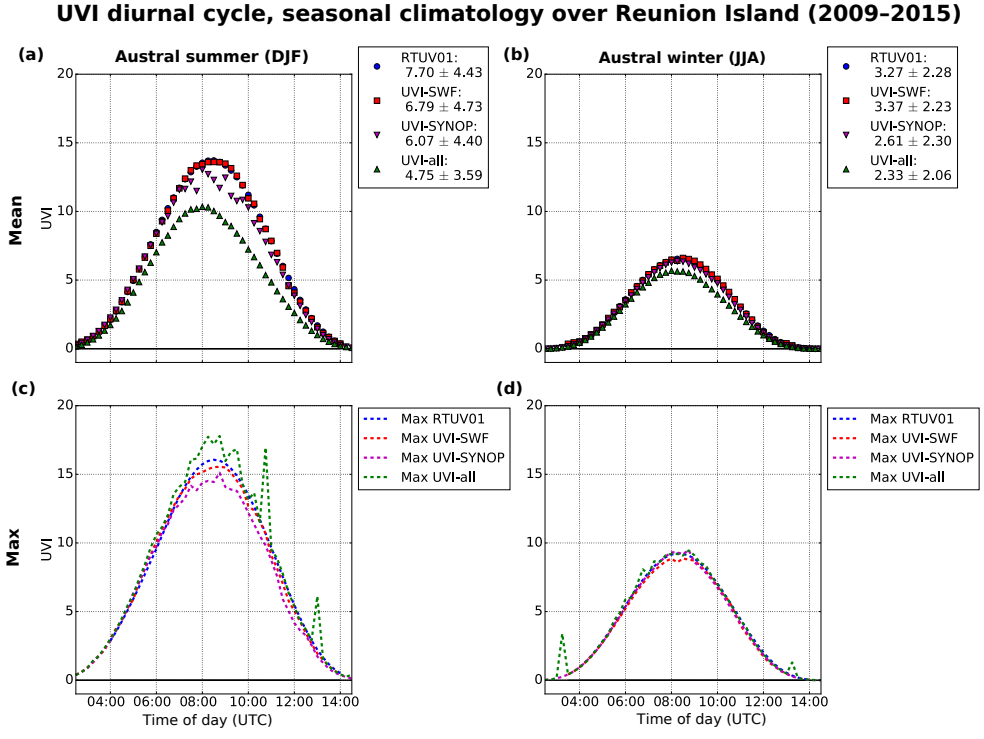

Figure 11. UVI diurnal cycle, seasonal climatology. Mean diurnal UVI on the top row and maximum diurnal UVI on the bottom row. Austral summer on the left side and austral winter on the right. RTUV01 in blue, UVI-SWF in red, UVI-SYNOP in purple and UVI-ALL in green.

ferent extraterrestrial spectra or ozone cross sections has not been investigated previously. For the extraterrestrial spectrum, we found a relative difference between 2.7 and 3.5 % depending on the total ozone column and solar zenith angle. For the ozone cross sections, the relative difference ranged from 2.4 to 2.9 %, also with a dependency on total ozone column and solar zenith angle.

The impact was higher for low solar zenith angle and low total ozone column during the diurnal and seasonal maximum of UVI, i.e. when the burning efficiency of the radia-

tion on human skin is higher. This difference was found to be dependent on the ozone and temperature profile.

For total ozone column and aerosols, the results were close to those of other studies carried out at different latitudes (Badosa et al., 2007). Badosa et al. (2007) also investigated the impact of ozone total column and aerosol optical thickness for four different sites: Lauder, New Zealand (45.04° S, 169.68° E); Boulder, Colorado (40.01° N, 105.25° W); Mauna Loa, Hawaii (19.53° N, 155.58° W); and Melbourne, Australia (37.69° S, 144.95° E). They found that different sources of input for total ozone column (SBUV or TOMS satellite measurements or Dobson ground measurements) had an impact of ~ 2 to 5 % on the surface UVI modelled. Here we found monthly mean differences between -2.5 and 7.5 % (Fig. 4). The mean difference in UVI sensitivity to the total ozone column was smaller than 0.4 % between any two data sets. UVI RTUV01 (SAOZ) was higher than RTUV02 (OMTO3). OMTO3 was on average the lowest total ozone column, which led to the highest modelled values of UVI. Brogniez et al. (2016) found that OMI-UVI products were higher than local measurements of UVI on Reunion Island with a mean relative bias of about 2 % and median relative bias of 4 %. OMI-UVI products are based on the OMTO3 product, but also take other OMI products (aerosols, surface albedo) into account (Krotkov et al., 2002). Here, using OMTO3 as the only input parameter to retrieve UVI did not produce a strong positive bias. Following the same study for aerosol (Badosa et al., 2007), it was found that AOT was very low at Mauna Loa, with values centred around 0.08, and the ratio between UVI modelled with and without aerosol was always between 0.96 and 1.02. Here, we found small mean differences between UVI modelled using daily measurements and monthly climatological values of AOT (about -0.40 %), but strong peaks in AOT could be missed and would yield UVI overestimations of ~ 30 %. Aerosol monthly climatology could be used for climatic studies of surface UVI but should be avoided for short-term predictions and preventive action for the population concerned, especially during the biomass burning season.

We also investigated the relationship between total ozone column and UVI variations through the radiative amplification factor (from a linear and a power law). At a SZA of 25° for the observations (UVI-SWF), model (RTUV07) and idealised model (i-RTUV), RAF_L of respectively 1.23, 1.34 and 1.34 was found. At a higher SZA, 60° lower RAF_L were found at 1.02, 1.16 and 1.23. RAF_P was higher than in other studies (Booth and Madronich, 1994; Herman, 2010) but these were done at higher latitudes. Here we found a RAF_P of 1.65 ± 0.12 for UVI-SWF at a SZA of 45°. Bodhaine et al. (1997) found 1.38 ± 0.2 for a similar site in the tropics. In general RAF tends to decrease as SZA increases. The significant dispersions on the observations make it impossible to make conclusions on the linear or power relation between total ozone column and UVI.

As previously noted, RAF tends to decrease as SZA increases, presumably because of various effects such as the influence of ozone, temperature profiles and Rayleigh scattering, which would reduce the impact of TO_3 on UVI.

Clear-sky UVI in the southern tropics was modelled with a MRD of 0.43 ± 5.83 up to 4.38 ± 5.78 % when comparing to ground-based measurements, which is within the modelling uncertainty of 5 %. MED values ranged from 0.44 to 4.51 %.

Monthly climatology of filtered and unfiltered clear-sky conditions revealed a few maximum values of UVI during all-sky conditions. This phenomenon is due to multiple reflections on cloud edges in the case of broken cloud cover.

Future study will be needed to take this into account. TUV is a one-dimensional model, but to considerer backscattering we need to have at least two-dimensional radiative transfer modelling. Following these results, the next step will be a projection of UV changes in the southern tropics.

Data availability. The data sets generated and/or analysed during the current study are available from the corresponding author on request.

The Supplement related to this article is available online at https://doi.org/10.5194/acp-18-227-2018-supplement.

Competing interests. The authors declare that they have no conflict of interest.

Special issue statement. This article is part of the special issue "Quadrennial Ozone Symposium 2016 – Status and trends of atmospheric ozone (ACP/AMT inter-journal SI)". It is a result of the Quadrennial Ozone Symposium 2016, Edinburgh, United Kingdom, 4–9 Sep 2016.

Acknowledgements. The authors acknowledge the Région Réunion, CNRS and Université de la Réunion for support and contribution within the research infrastructure OPAR (Observatoire de Physique de l'Atmosphère à la Réunion). OPAR is currently funded by CNRS (INSU) and Université de la Réunion and managed by OSU-R (Observatoires des Sciences de l'Univers à la Réunion, UMS 3365). The authors acknowledge Photon Aeronet and the NDACC network for the aerosols and ozone data. Marcel Dobber (KNMI, NL) is acknowledged for providing the Dobber et al. (2008) extraterrestrial solar spectrum.

Edited by: Stelios Kazadzis
Reviewed by: two anonymous referees

References

Badosa, J., McKenzie, R. L., Kotkamp, M., Calbó, J., González, J. A., Johnston, P. V., O'Neill, M., and Anderson, D. J.: Towards closure between measured and modelled UV under clear skies at four diverse sites, Atmos. Chem. Phys., 7, 2817–2837, https://doi.org/10.5194/acp-7-2817-2007, 2007.

Bais, A. F., Zerefos, C. S., Meleti, C., Ziomas, I. C., and Tourpali, K.: Spectral measurements of solar UVB radiation and its relations to total ozone, SO_2, and clouds, J. Geophys. Res.-Atmos., 98, 5199–5204, https://doi.org/10.1029/92JD02904, 1993.

Bais, A. F., Tourpali, K., Kazantzidis, A., Akiyoshi, H., Bekki, S., Braesicke, P., Chipperfield, M. P., Dameris, M., Eyring, V., Garny, H., Iachetti, D., Jöckel, P., Kubin, A., Langematz, U., Mancini, E., Michou, M., Morgenstern, O., Nakamura, T., Newman, P. A., Pitari, G., Plummer, D. A., Rozanov, E., Shepherd, T. G., Shibata, K., Tian, W., and Yamashita, Y.: Projections of UV radiation changes in the 21st century: impact of ozone recovery and cloud effects, Atmos. Chem. Phys., 11, 7533–7545, https://doi.org/10.5194/acp-11-7533-2011, 2011.

Bais, A. F., McKenzie, R. L., Bernhard, G., Aucamp, P. J., Ilyas, M., Madronich, S., and Tourpali, K.: Ozone depletion and climate change: Impacts on UV radiation, Photochem. Photobio. S., 14, 19–52, https://doi.org/10.1039/c4pp90032d, 2015.

Baldy, S., Ancellet, G., Bessafi, M., Badr, A., and Luk, D. L. S.: Field observations of the vertical distribution of tropospheric ozone at the island of Reunion (southern tropics), J. Geophys. Res.-Atmos., 101, 23835–23849, https://doi.org/10.1029/95jd02929, 1996.

Bass, A. M. and Paur, R. J.: The ultraviolet cross-sections of ozone. I. The measurements. II – Results and temperature dependence, in: Atmospheric ozone; Proceedings of the Quadrennial, edited by: Zerefos, C. S. and Ghazi, A., 606–616, Springer Netherlands, Dordrecht, the Netherlands, 1985.

Bhartia, P. K. and Wellemeyer, C.: TOMS-V8 total O_3 algorithm, OMI Algorithm Theoretical Basis Document, 2, 15–31, 2002.

Bodhaine, B. A., Dutton, E. G., Hofmann, D. J., McKenzie, R. L., and Johnston, P. V.: UV measurements at Mauna Loa: July 1995 to July 1996, J. Geophys. Res.-Atmos., 102, 19265–19273, https://doi.org/10.1029/97jd01391, 1997.

Booth, C. R. and Madronich, S.: Radiation amplification factors: Improved formulation accounts for large increases in ultraviolet radiation associated with Antarctic ozone depletion, in: Ultraviolet Radiation in Antarctica: Measurements and Biological Effects, edited by: Weiler, C. S. and Penhale, P. A., American Geophysical Union, Washington, D. C., https://doi.org/10.1029/AR062p0039, 1994.

Boucher, O., Randall, D., Artaxo, P., Bretherton, C., Feingold, G., Forster, P., Kerminen, V.-M., Kondo, Y., Liao, H., Lohmann, U., Rasch, P., Satheesh, S., Sherwood, S., Stevens, B., and Zhang, X.: Clouds and Aerosols, climate change 2013: the physical science basis. contribution of working group i to the fifth assessment report of the intergovernmental panel on climate change, section 7, Cambridge University Press, Cambridge, UK and New York, NY, USA, 571–658, https://doi.org/10.1017/CBO9781107415324.016, 2013.

Brion, J., Chakir, A., Charbonnier, J., Daumont, D., Parisse, C., and Malicet, J.: Absorption spectra measurements for the ozone molecule in the 350–830 nm region, J. Atmos. Chem., 30, 291–299, 1998.

Brogniez, C., Auriol, F., Deroo, C., Arola, A., Kujanpää, J., Sauvage, B., Kalakoski, N., Pitkänen, M. R. A., Catalfamo, M., Metzger, J.-M., Tournois, G., and Da Conceicao, P.: Validation of satellite-based noontime UVI with NDACC ground-based instruments: influence of topography, environment and satellite overpass time, Atmos. Chem. Phys., 16, 15049–15074, https://doi.org/10.5194/acp-16-15049-2016, 2016.

Brühl, C. and Crutzen, P. J.: On the disproportionate role of tropospheric ozone as a filter against solar UV-B radiation, Geophys. Res. Lett., 16, 703–706, https://doi.org/10.1029/GL016i007p00703, 1989.

Butchart, N.: The Brewer-Dobson circulation, Rev. Geophys., 52, 157–184, https://doi.org/10.1002/2013rg000448, 2014.

Butler, A. H., Daniel, J. S., Portmann, R. W., Ravishankara, A. R., Young, P. J., Fahey, D. W., and Rosenlof, K. H.: Diverse policy implications for future ozone and surface UV in a changing climate, Environ. Res. Lett., 11, 064017, https://doi.org/10.1088/1748-9326/11/6/064017, 2016.

Calbó, J., Pagès, D., and González, J.-A.: Empirical studies of cloud effects on UV radiation: A review, Rev. Geophys., 43, RG2002, https://doi.org/10.1029/2004RG000155, 2005.

Cede, A., Blumthaler, M., Luccini, E., Piacentini, R. D., and Nuñez, L.: Effects of clouds on erythemal and total irradiance as derived from data of the Argentine Network, Geophys. Res. Lett., 29, 76-1–76-4, https://doi.org/10.1029/2002gl015708, 2002.

Chance, K. and Kurucz, R.: An improved high-resolution solar reference spectrum for earth's atmosphere measurements in the ultraviolet, visible, and near infrared, J. Quant. Spectrosc. Ra., 111, 1289–1295, 2010.

Commission Internationale de l'Eclairage: CIE STANDARD: Erythema Reference Action Spectrum and Standard Erythema Dose, CIE S007E-1998, CIE Central Bureau, Vienna, Austria, 1998.

Correa, M. d. P., Godin-Beekmann, S., Haeffelin, M., Bekki, S., Saiag, P., Badosa, J., Jegou, F., Pazmino, A., and Mahe, E.: Projected changes in clear-sky erythemal and vitamin D effective UV doses for Europe over the period 2006 to 2100, Photochem. Photobio. S., 12, 1053–1064, https://doi.org/10.1039/C3PP50024A, 2013.

Dobber, M., Voors, R., Dirksen, R., Kleipool, Q., and Levelt, P.: The high-resolution solar reference spectrum between 250 and 550 nm and its application to measurements with the Ozone Monitoring Instrument, Sol. Phys., 249, 281–291, 2008.

Dubovik, O., Smirnov, A., Holben, B. N., King, M. D., Kaufman, Y. J., Eck, T. F., and Slutsker, I.: Accuracy assessments of aerosol optical properties retrieved from Aerosol Robotic Network (AERONET) Sun and sky radiance measurements, J. Geophys. Res.-Atmos., 105, 9791–9806, https://doi.org/10.1029/2000jd900040, 2000.

Elterman, L.: UV, Visible, and IR Attenuation for Altitudes to 50 km, 1968, Tech. rep., DTIC Document, Environmental Research Paper No. 285, Air Force Cambridge Research Laboratories, Hanscom Air Force Base, 1968.

Erickson III, D. J., Sulzberger, B., Zepp, R. G., and Austin, A. T.: Effects of stratospheric ozone depletion, solar UV radiation, and climate change on biogeochemical cycling: interactions and feedbacks, Photochem. Photobio. S., 14, 127–148, https://doi.org/10.1039/C4PP90036G, 2015.

Froidevaux, L., Jiang, Y. B., Lambert, A., Livesey, N. J., Read, W. G., Waters, J. W., Browell, E. V., Hair, J. W., Avery, M. A.,

McGee, T. J., Twigg, L. W., Sumnicht, G. K., Jucks, K. W., Margitan, J. J., Sen, B., Stachnik, R. A., Toon, G. C., Bernath, P. F., Boone, C. D., Walker, K. A., Filipiak, M. J., Harwood, R. S., Fuller, R. A., Manney, G. L., Schwartz, M. J., Daffer, W. H., Drouin, B. J., Cofield, R. E., Cuddy, D. T., Jarnot, R. F., Knosp, B. W., Perun, V. S., Snyder, W. V., Stek, P. C., Thurstans, R. P., and Wagner, P. A.: Validation of Aura Microwave Limb Sounder stratospheric ozone measurements, J. Geophys. Res., 113, D15S20, https://doi.org/10.1029/2007jd008771, 2008.

Gorshelev, V., Serdyuchenko, A., Weber, M., Chehade, W., and Burrows, J. P.: High spectral resolution ozone absorption cross-sections – Part 1: Measurements, data analysis and comparison with previous measurements around 293 K, Atmos. Meas. Tech., 7, 609–624, https://doi.org/10.5194/amt-7-609-2014, 2014.

Hader, D.-P., Kumar, H. D., Smith, R. C., and Worrest, R. C.: Effects of solar UV radiation on aquatic ecosystems and interactions with climate change, Photochem. Photobio. S., 6, 267–285, https://doi.org/10.1039/B700020K, 2007.

Hegglin, M. I. and Shepherd, T. G.: Large climate-induced changes in ultraviolet index and stratosphere-to-troposphere ozone flux, Nat. Geosci., 2, 687–691, https://doi.org/10.1038/ngeo604, 2009.

Herman, J. R.: Use of an improved radiation amplification factor to estimate the effect of total ozone changes on action spectrum weighted irradiances and an instrument response function, J. Geophys. Res., 115, D23119, https://doi.org/10.1029/2010jd014317, 2010.

Herman, J. R., Bhartia, P. K., Torres, O., Hsu, C., Seftor, C., and Celarier, E.: Global distribution of UV-absorbing aerosols from Nimbus 7/TOMS data, J. Geophys. Res.-Atmos., 102, 16911–16922, https://doi.org/10.1029/96JD03680, 1997.

Holick, M. F., MacLaughlin, J., Clark, M., Holick, S., Potts, J., Anderson, R., Blank, I., Parrish, J., and Elias, P.: Photosynthesis of previtamin D3 in human skin and the physiologic consequences, Science, 210, 203–205, 1980.

Jégou, F., Godin-Beekman, S., Corrêa, M. P., Brogniez, C., Auriol, F., Peuch, V. H., Haeffelin, M., Pazmino, A., Saiag, P., Goutail, F., and Mahé, E.: Validity of satellite measurements used for the monitoring of UV radiation risk on health, Atmos. Chem. Phys., 11, 13377–13394, https://doi.org/10.5194/acp-11-13377-2011, 2011.

Kazadzis, S., Kouremeti, N., Bais, A., Kazantzidis, A., and Meleti, C.: Aerosol forcing efficiency in the UVA region from spectral solar irradiance measurements at an urban environment, Ann. Geophys., 27, 2515–2522, https://doi.org/10.5194/angeo-27-2515-2009, 2009.

Koelemeijer, R., De Haan, J., and Stammes, P.: A database of spectral surface reflectivity in the range 335–772 nm derived from 5.5 years of GOME observations, J. Geophys. Res.-Atmos., 108, 4070, https://doi.org/10.1029/2002JD002429, 2003.

Koepke, P., Bais, A., Balis, D., Buchwitz, M., Backer, H., Cabo, X., Eckert, P., Eriksen, P., Gillotay, D., Heikkilä, A., Koskela, T., Lapeta, B., Litynska, Z., Lorente, J., Mayer, B., Renaud, A., Ruggaber, A., Schauberger, G., Seckmeyer, G., Seifert, P., Schmalwieser, A., Schwander, H., Vanicek, K., and Weber, M.: Comparison of models used for UV index calculations, Photochem. Photobiol., 67, 657–662, 1998.

Krotkov, N. A., Herman, J., Bhartia, P. K., Seftor, C., Arola, A., Kaurola, J., Taalas, P., and Vasilkov, A.: OMI Surface UV Irradiance Algorithm, in: OMI Algorithm Theoretical Basis Document, Volume III: Clouds, Aerosols, and Surface UV Irradiance, ATBD-OMI-03, NASA Goddard Space Flight Center, Greenbelt, Maryland, USA, 2002.

Krzyścin, J. W. and Puchalski, S.: Aerosol impact on the surface UV radiation from the ground-based measurements taken at Belsk, Poland, 1980–1996, J. Geophys. Res.-Atmos., 103, 16175–16181, https://doi.org/10.1029/98JD00899, 1998.

Lacagnina, C., Hasekamp, O. P., Bian, H., Curci, G., Myhre, G., van Noije, T., Schulz, M., Skeie, R. B., Takemura, T., and Zhang, K.: Aerosol single-scattering albedo over the global oceans: Comparing PARASOL retrievals with AERONET, OMI, and AeroCom models estimates, J. Geophys. Res.-Atmos., 120, 9814–9836, https://doi.org/10.1002/2015jd023501, 2015.

Lee-Taylor, J., Madronich, S., Fischer, C., and Mayer, B.: A Climatology of UV Radiation, 1979–2000, 65S–65N, UV Radiation in Global Climate Change, Springer Berlin Heidelberg, 1–20, https://doi.org/10.1007/978-3-642-03313-1_1, 2010.

Long, C. N. and Ackerman, T. P.: Identification of clear skies from broadband pyranometer measurements and calculation of downwelling shortwave cloud effects, J. Geophys. Res.-Atmos., 105, 15609–15626, 2000.

Long, C. N., Ackerman, T. P., Gaustad, K. L., and Cole, J.: Estimation of fractional sky cover from broadband shortwave radiometer measurements, J. Geophys. Res.-Atmos., 111, D11204, https://doi.org/10.1029/2005JD006475, 2006.

MacLaughlin, J. A., Anderson, R., and Holick, M. F.: Spectral character of sunlight modulates photosynthesis of previtamin D3 and its photoisomers in human skin, Science, 216, 1001–1003, 1982.

Madronich, S.: UV radiation in the natural and perturbed atmosphere, Lewis Publisher, Boca Raton, USA, 1993.

Mahé, E., Beauchet, A., de Paula Corrêa, M., Godin-Beekmann, S., Haeffelin, M., Bruant, S., Fay-Chatelard, F., Jégou, F., Saiag, P., and Aegerter, P.: Outdoor sports and risk of ultraviolet radiation-related skin lesions in children: Evaluation of risks and prevention., Brit. J. Dermatol., 165, 360–367, https://doi.org/10.1111/j.1365-2133.2011.10415.x, 2011.

Mahé, E., Corrêa, M. P., Godin-Beekmann, S., Haeffelin, M., Jégou, F., Saiag, P., and Beauchet, A.: Evaluation of tourists' UV exposure in Paris., J. Eur. Acad. Dermatol., 27, 294–304, https://doi.org/10.1111/j.1468-3083.2012.04637.x, 2013.

Malicet, J., Daumont, D., Charbonnier, J., Parisse, C., Chakir, A., and Brion, J.: Ozone UV spectroscopy. II. Absorption cross-sections and temperature dependence, J. Atmos. Chem., 21, 263–273, 1995.

Matsumura, Y. and Ananthaswamy, H. N.: Toxic effects of ultraviolet radiation on the skin, Toxicol. Appl. Pharm., 195, 298–308, 2004.

Mayer, B., Kylling, A., Madronich, S., and Seckmeyer, G.: Enhanced absorption of UV radiation due to multiple scattering in clouds: Experimental evidence and theoretical explanation, J. Geophys. Res.-Atmos., 103, 31241–31254, https://doi.org/10.1029/98JD02676, 1998.

McKenzie, R. L., Matthews, W. A., and Johnston, P. V.: The relationship between erythemal UV and ozone, derived from spectral irradiance measurements, Geophys. Res. Lett., 18, 2269–2272, https://doi.org/10.1029/91GL02786, 1991.

McKenzie, R. L., Liley, J. B., and Björn, L. O.: UV radiation: balancing risks and benefits, Photochem. Photobiol., 85, 88–98, 2009.

McKenzie, R. L., Aucamp, P. J., Bais, A. F., Björn, L. O., Ilyas, M., and Madronich, S.: Ozone depletion and climate change: impacts on UV radiation, Photochem. Photobio. S., 10, 182–198, https://doi.org/10.1039/c0pp90034f, 2011.

McKinlay, A. F. and Diffey, B. L.: A reference action spectrum for ultraviolet induced erythema in human skin, CIE J, 6, 17–22, 1987.

McPeters, R. D. and Labow, G. J.: Climatology 2011: An MLS and sonde derived ozone climatology for satellite retrieval algorithms, J. Geophys. Res.-Atmos., 117, D10303, https://doi.org/10.1029/2011JD017006, 2012.

Morgenstern, O., Braesicke, P., Hurwitz, M. M., O'Connor, F. M., Bushell, A. C., Johnson, C. E., and Pyle, J. A.: The World Avoided by the Montreal Protocol, Geophys. Res. Lett., 35, L16811, https://doi.org/10.1029/2008GL034590, 2008.

Newman, P. A., Oman, L. D., Douglass, A. R., Fleming, E. L., Frith, S. M., Hurwitz, M. M., Kawa, S. R., Jackman, C. H., Krotkov, N. A., Nash, E. R., Nielsen, J. E., Pawson, S., Stolarski, R. S., and Velders, G. J. M.: What would have happened to the ozone layer if chlorofluorocarbons (CFCs) had not been regulated?, Atmos. Chem. Phys., 9, 2113–2128, https://doi.org/10.5194/acp-9-2113-2009, 2009.

Orphal, J., Staehelin, J., Tamminen, J., et al.: Absorption cross-sections of ozone in the ultraviolet and visible spectral regions: Status report 2015, J. Mol. Spectrosc., 327, 105–121, https://doi.org/10.1016/j.jms.2016.07.007, 2016.

Petropavlovskikh, I. and Brasseur, G.: Evaluation of photodissociation coefficient calculations for use in atmospheric chemical models, PhD Thesis, University of Brussels and NCAR/CT-159, Boulder, USA, 1995.

Pommereau, J. P. and Goutail, F.: O_3 and NO_2 ground-based measurements by visible spectrometry during Arctic winter and spring 1988, Geophys. Res. Lett., 15, 891–894, https://doi.org/10.1029/gl015i008p00891, 1988.

Serdyuchenko, A., Gorshelev, V., Weber, M., Chehade, W., and Burrows, J. P.: High spectral resolution ozone absorption cross-sections – Part 2: Temperature dependence, Atmos. Meas. Tech., 7, 625–636, https://doi.org/10.5194/amt-7-625-2014, 2014.

Smith, R. C. and Cullen, J. J.: Effects of UV radiation on phytoplankton, Rev. Geophys., 33, 1211–1223, https://doi.org/10.1029/95RG00801, 1995.

Stamnes, K., Tsay, S.-C., Wiscombe, W., and Jayaweera, K.: Numerically stable algorithm for discrete-ordinate-method radiative transfer in multiple scattering and emitting layered media, Appl. Optics, 27, 2502–2509, 1988.

Takemura, T., Nakajima, T., Dubovik, O., Holben, B. N., and Kinne, S.: Single-Scattering Albedo and Radiative Forcing of Various Aerosol Species with a Global Three-Dimensional Model, J. Climate, 15, 333–352, https://doi.org/10.1175/1520-0442(2002)015<0333:ssaarf>2.0.co;2, 2002.

Toon, O. B., McKay, C., Ackerman, T., and Santhanam, K.: Rapid calculation of radiative heating rates and photodissociation rates in inhomogeneous multiple scattering atmospheres, J. Geophys. Res.-Atmos., 94, 16287–16301, 1989.

van Dijk, A., Slaper, H., den Outer, P. N., Morgenstern, O., Braesicke, P., Pyle, J. A., Garny, H., Stenke, A., Dameris, M., Kazantzidis, A., Tourpali, K. and Bais, A.: Skin Cancer Risks Avoided by the Montreal Protocol – Worldwide Modeling Integrating Coupled Climate-Chemistry Models with a Risk Model for UV, Photochem. Photobiol., 89, 234–246, 2013.

WHO: Global solar UV index: a practical guide, in: Global Solar UV Index, World Health Organization, Geneva, Switzerland, 2002.

Willson, R. C. and Hudson, H. S.: The Sun's luminosity over a complete solar cycle, Nature, 351, 42–44, 1991.

WMO: Scientific Assessment of Ozone Depletion: 2014, in: Scientific Assessment of Ozone Depletion: 2014, 55, p. 416, Geneva, Switzerland, 2014.

Wright, C. Y., Reeder, A. I., Bodeker, G. E., Gray, A., and Cox, B.: Solar UVR Exposure, Concurrent Activities and Sun-Protective Practices Among Primary Schoolchildren, Photochem. Photobiol., 83, 749–758, https://doi.org/10.1562/2006-08-22-ra-1010, 2007.

Wright, C. Y., Brogniez, C., Ncongwane, K. P., Sivakumar, V., Coetzee, G., Metzger, J.-M., Auriol, F., Deroo, C., and Sauvage, B.: Sunburn Risk Among Children and Outdoor Workers in South Africa and Reunion Island Coastal Sites, Photochem. Photobiol., 89, 1226–1233, https://doi.org/10.1111/php.12123, 2013.

Zepp, R. G., Erickson III, D. J., Paul, N. D., and Sulzberger, B.: Interactive effects of solar UV radiation and climate change on biogeochemical cycling, Photochem. Photobio. S., 6, 286–300, https://doi.org/10.1039/B700021A, 2007.